AN INTEGRATED AND SYSTEMATIC CHARACTERIZATION METHODOLOGY FOR VACUUM BAG ONLY PREPREGS

by
MUHAMMED HASAN ARIKAN

Submitted to the Graduate School of Engineering
in partial fulfilment of
the requirements for the degree of Master of Science

Sabancı University
September 2020

AN INTEGRATED AND SYSTEMATIC CHARACTERIZATION METHODOLOGY FOR VACUUM BAG ONLY PREPREGS

Approved by:

Asst. Prof. Dr. Hatice Sinem Şaş .....
(Thesis Supervisor)

Assoc. Prof. Dr. Volkan Eskizeybek .....

Prof. Dr. Mehmet Yıldız .....

Date of Approval: September 7, 2020

ABSTRACT

AN INTEGRATED AND SYSTEMATIC CHARACTERIZATION METHODOLOGY FOR VACUUM BAG ONLY PREPREGS

MUHAMMED HASAN ARIKAN

MANUFACTURING ENGINEERING M.SC. THESIS, SEPTEMBER 2020

Thesis Supervisor: Asst. Prof. Dr. Hatice Sinem Şaş

Keywords: Advanced composites, out-of-autoclave processing, vacuum bag only prepregs, characterization, process modeling

Composite materials have attracted widespread acceptance aerospace industry in the last decades as it offers high rigidity and outstanding strength/weight ratio while enabling the considerable reductions in the manufacturing and operational costs. The autoclave processes have been widely preferred for the primary and secondary aerospace applications as such requirements as high safety, high quality, and reproducibility of the industry. However, producing larger composite parts through low-cost processes has led the industry to out of autoclave processes. Hence, VBO prepregs were developed for out-of-autoclave processes to deliver high-performance composites, which can compete with the autoclave-quality composites in many aspects, such as low-void content and successful impregnation. This is possible through an appropriate combination of fiber bed architecture and resin system, and process parameters. However, composites produced through VBO prepregs are much more susceptible to voids since the maximum consolidation pressure is limited to atmospheric pressure. To address these issues, VBO prepregs were designed to incorporate relatively permeable air channels and exhibit higher initial fiber volume fractions in comparison with the autoclave prepreg systems. Nevertheless, the physical properties of the prepreg system are still the leading parameters in the evolution of VBO prepreg microstructures during the curing process as the incomplete impregnation before gelation directly controls the amount of voids, which degrades the mechanical performance of the final part.

Therefore, there is a vital need for a systematic and overarching characterization

methodology. This thesis aims to establish a methodology that systematically characterizes such factors as material properties and constitutive behavior to strengthen the VBO prepreg process model's accuracy and reliability. To achieve this goal, a systematic was developed to characterize the main properties of the resin and prepreg system. This approach was also implemented to characterize a commercial VBO prepreg system's properties and processing parameters.

Hence, the cure-dependent properties of the resin system were characterized by several sets of semi-empirical phenomenological models. Then, the first fiber architecture, void-content change, the fiber volume fraction of the prepreg system were investigated through sets of x-ray microtomography scans of the prepreg laminates. The initial permeability behavior of the porous media was modeled through a CFD analysis. Finally, the specific heat capacity and thermal conductivity of the constituents were investigated by a series of experiments and numerical studies.

This approach can be accepted as a fundamental cornerstone of establishing a process design that integrates characterization, modeling, optimization, and verification approaches to deliver high-performance composites through OoA techniques.

ÖZET

VAKUM TORBALAMA PREPREG SİSTEMLERİ İÇİN ENTEGRE VE SİSTEMATİK KARAKTERİZASYON METODOLOJİSİ

MUHAMMED HASAN ARIKAN

ÜRETİM MÜHENDİSLİĞİ YÜKSEK LİSANS TEZİ, EYLÜL 2020

Tez Danışmanı: Asst. Prof. Dr. Hatice Sinem Şaş

Anahtar Kelimeler: İleri kompozitler, otoklav-dışı prosesler, vakum torbalama prepregleri, karakterizasyon, proses modelleme

Otoklav dışı prosesler için geliştirilen vakum torbalama prepregler, fiber yatağı mimarisi ve reçine sistemi ve proses parametrelerinin uygun bir kombinasyonu yoluyla düşük boşluk içeriği ve reçinenin kuru fiber demetlerine başarılı emdirilmesi gibi birçok açıdan otoklav kalitesinde kompozit yapılar elde edebilir. Öte yandan, maksimum konsolidasyon basıncı atmosferik basınçla sınırlı olduğundan dolayı gözeneklilik ve malzeme içi boşluklar vakum torbalama prosesleri ile ilgili en zorlu konulardır. Bu sorunları gidermek için, vakum torbalama prepregleri nispeten geçirgen hava kanallarını içerecek ve otoklav prepreg sistemlerine kıyasla daha yüksek başlangıç fiber hacmi fraksiyonları sergileyecek şekilde tasarlanmaktadır. Buna rağmen, jelleşme öncesi tamamlanmamış emdirme işlemi, nihai parçanın mekanik performansını düşüren boşlukların miktarını doğrudan kontrol ettiğinden, prepreg sisteminin fiziksel özellikleri, kürlenme işlemi sırasında vakum torbalama prepregleri ile üretilen kompozitlerin mikro yapılarının evriminde hala önde gelen parametrelerdir.

Kompozit malzemeler, yüksek sertlik ve başarılı güç/ağırlık oranı sunarken aynı zamanda üretim ve proses maliyetlerinde önemli düşüşler sağladığından dolayı son yıllarda havacılık endüstrisinde yaygın kabul görmüştür. Otoklav prosesleri, endüstrinin yüksek güvenlik, yüksek kalite ve tekrar üretilebilirlik gibi gereklilikleri başarıyla yerine getirebildiği için birincil ve ikincil havacılık uygulamaları için yaygın olarak tercih edilmiştir. Ancak, düşük maliyetli süreçlerle daha büyük kompozit parçalar üretmek, endüstrinin otoklav-dışı proses arayışlarına yönelmesine neden olmuştur. Bu nedenle, VBO prepregleri, düşük boşluk içeriği ve reçinenin başarılı

emdirilmesi gibi birçok konuda otoklav kalitesinde kompozitler ile rekabet edebilen yüksek performanslı kompozitler sağlamak üzere otoklav-dışı prosesler için geliştirilmiştir. Bu, uygun bir elyaf yatağı mimarisi, reçine sistemi ve proses parametreleri kombinasyonu ile mümkündür. Bununla birlikte, maksimum konsolidasyon basıncı atmosferik basınçla sınırlı olduğu için VBO prepreglerinden üretilen kompozitler boşluklara çok daha duyarlıdır. Bu sorunları gidermek için, VBO prepregleri nispeten geçirgen hava kanallarını içerecek ve otoklav prepreg sistemlerine kıyasla daha yüksek başlangıç fiber hacmi fraksiyonlarına sahip olacak şekilde tasarlanmıştır. Bununla birlikte, jelleşme öncesi tamamlanmamış emdirme, nihai parçanın mekanik performansını düşüren boşlukların miktarını doğrudan kontrol ettiğinden dolayı prepreg sisteminin fiziksel özellikleri, kürlenme prosesi sırasında VBO prepreg mikro yapılarının evriminde hala önde gelen parametrelerdir.

Bu nedenle, sistematik ve kapsayıcı bir karakterizasyon metodolojisine hayati bir ihtiyaç vardır. Bu tez, vakum torbalama prepregleri proses modelinin doğruluğunu ve güvenilirliğini güçlendirmek için malzeme özellikleri ve yapısal davranış gibi faktörleri sistematik olarak karakterize eden bir metodoloji oluşturmayı amaçlamaktadır. Bu amaca ulaşmak için reçine ve prepreg sisteminin temel özelliklerini karakterize eden bir sistematik geliştirilmiştir. Bu yaklaşım, ticari bir VBO prepreg sisteminin özelliklerini ve proses parametrelerini karakterize etmek için de uygulanmıştır.

Bu nedenle, reçine sisteminin kürlenmeye bağlı özellikleri, birkaç grup yarı-deneysel fenomenolojik modeller aracığılıyla karakterize edilmiştir. Ardından, ilk fiber mimarisi, boşluk içeriği değişimi, prepreg sisteminin fiber hacim fraksiyonu, prepreg laminatlarının x-ışını mikrotomografi taraması setleriyle incelenmiştir. Gözenekli ortamın ilk geçirgenlik davranışı, bir hesaplamalı akışkanlar dinamiği analizi ile modellenmiştir. Son olarak, bileşenlerin ve bütüncül olarak sistemin özgül ısı kapasitesi ve ısıl iletkenliği, bir dizi deney ve nümerik çalışma ile karakterize edilmiştir.

Bu yaklaşım, OoA teknikleri aracılığıyla yüksek performanslı kompozitler sunmak için karakterizasyon, modelleme, optimizasyon ve doğrulama yaklaşımlarını bütünleştiren bir proses tasarımı oluşturmanın temel bir köşe taşı olarak kabul edilebilir.

ACKNOWLEDGEMENTS

First, I would like to express my sincerest gratitude to my research supervisor, Asst. Prof. Dr. Hatice Sinem Şaş Çaycı, for the valuable supervision I received and her continuous support during my master's degree.

This work was performed with support by the Scientific and Technological Research Council of Turkey (TÜBİTAK) under the Grant No. 118M625. Support was also given by the Sabancı University and Kordsa, who funded the work in all its stages. I would like to acknowledge all the parties who made this project possible.

I am also indebted to Assoc. Prof. Dr. Volkan Eskizeybek who also guided me during my research for his much valuable advice.

I would also like to gratefully thank to Prof. Dr. Mehmet Yıldız, for his ongoing collaboration and great help in all stages of this research.

I would like to acknowledge my colleague, Fatih Eroğlu, who was always my closest collaborator in this work.

Personal thanks are also due to my dearest friends from Sabancı University: Bora Gönül, Hafiz Qasim Ali, Fatih Uzun, for their continuous help and constructive comments. Additionally, I would like to thank all Sabancı University Composite Technologies Center of Excellence members, specifically, staff at Material Characterization and Advanced Composite Manufacturing laboratories.

Last but not least, none of this would have been possible without my family's love and support.

Dedicated to my beloved family...

TABLE OF CONTENTS

LIST OF TABLES

LIST OF FIGURES

1. INTRODUCTION

Two fundamental needs stimulate the development of new generation structural materials for the aerospace industry: delivering more competent, durable, and reliable aircraft by advancing the material performance, and while doing this, reducing the cost of manufacturing and operation [1].

Composite materials have been introduced as a novel solution to these demands of the industry in the mid-1970s. Principally, composites are the materials consisting of two or more different materials whose combined performance outstrips that of the constituents. Predominantly for the aerospace primary and secondary structure applications, carbon fibers are preferred as the reinforcement material embedded inside an epoxy matrix to preserve the overall shape of the composite. Carbon fibers are the load-bearing materials in this engineered combination, while the epoxy transfers the loads between fibers and protects them from the degradation [2]. Altogether composites offer high rigidity, excellent strength/weight ratio, and relatively high endurance to environmental factors.

Composite materials' manufacturing is distinct from the traditional manufacturing of the aircraft's metallic structures. The composite material commonly comprises layers of semi-manufactured fiber forms, namely "prepregs", developed to deliver high-performance composites produced by impregnating the dry fiber batches with a predetermined amount of uncured resin to achieve a particular fiber volume ratio [3]. Prepreg systems have various forms in terms of weaving styles, such as unidirectional fibers or woven fabrics, reinforcement and matrix material compositions such as carbon-epoxy or glass-epoxy depending upon the application [2]. Processes involving prepregs generally incorporate four primary manufacturing steps: fabrication of the prepregs, laminating the prepreg plies, vacuum-bagging, and subsequent curing.

Hot-melting is a widely preferred process for fabricating the high-performance prepreg systems. The reason for this is that hot melt provides excellent flexibility for such process parameters as compaction force of the rollers while adjusting the heat subjected to both fiber bed and resin to obtain the best resin/fiber vol-

ume ratio [4]. Generally, a fabricated prepreg ply introduces about $30-40\%$ resin content by weight. Subsequently, prepreg is cut into the desired shape, placed on a mold, laminated with a number of prepreg plies to achieve manufacturer's desired thickness. Then, this prepreg arrangement is enclosed in a vacuum bag assembly to provide a pressure drop and subjected to curing at elevated temperatures and pressures [5].

This adjusting possibility makes composites manufacturing advantageous since it can be highly optimized. Composite manufacturing also allows integrated manufacturing of the large parts, while metallic aircraft structures of great sizes are traditionally built upon a large number of smaller pieces. This assembly process is so costly and time-consuming for some applications that it can account for almost 50% of the total airframe cost. Composites, therefore, can boost production by allowing the creation of large and integrated parts at once, which can lead to significant reductions in time and cost.

The use of composite materials in primary and secondary aerospace applications has dramatically escalated in the last decades. Boeing 787 Dreamliner, which features an airframe consisting of 50% composite materials by weight [4], and therefore, provides a 30% reduction in fuel consumption as a result of its extensively carbon-reinforced airframe structure. The manufacturing techniques used to produce the composite airframes are applicable to a wide range of models (like the 787), for which projected unit production demand results in a doubled world fleet by 2032 [4].

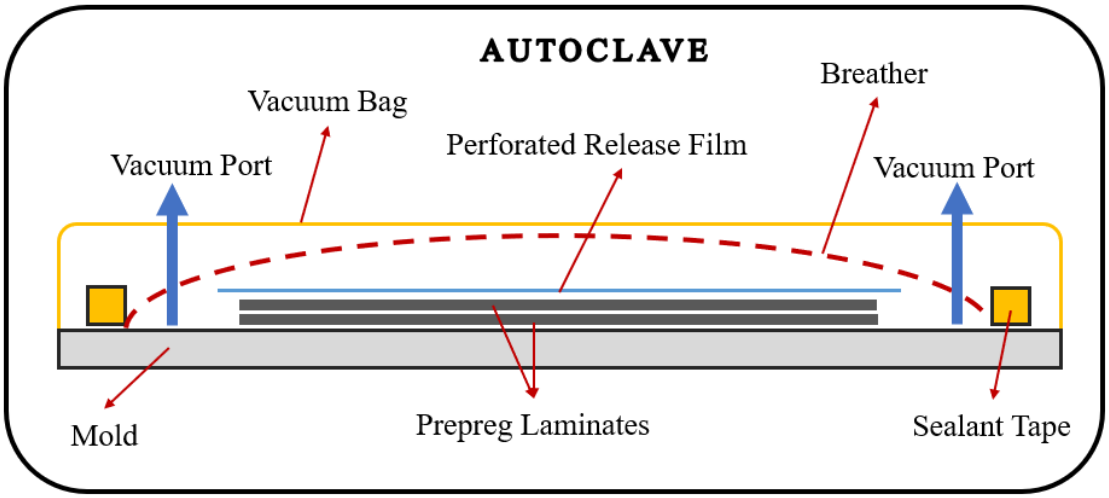

Figure 1.1 The schematic of a typical autoclave processing

As previously explained, the prepreg layers are initially cut and stacked to form a laminate. Then, this laminate is enclosed within a vacuum bag assembly and in-

stalled into the autoclave, as illustrated in Figure 1.1. The autoclave is simply a pressurized vessel with a cylindrical tube shape. Inside the autoclave, a pressure difference is applied; the pressure inside the vacuum bag is decreased so that the vacuum application is constituted, and separately the ambient pressure (within the autoclave) is raised (by up to a factor of six). Additionally, the ambient temperature is elevated to the desired temperature (up to 200℃) to decrease the resin's viscosity, thus, impregnating the dry-fiber bed and initiating the curing reaction. This pressure difference acts as a compaction force to consolidate the laminate to the final thickness and shape. It also allows the epoxy resin to flow into resin-poor areas and collapse gas bubbles resulted due to volatiles. The autoclave process has proved a remarkable success in reducing the void content of less than 1% by volume in the composite parts, which is one of the most critical criteria of the aerospace industry [2, 3]. This success is achieved by the rapid removal of air bubbles trapped within the part through high temperatures and high pressure during the process.

In addition to such requirements as high safety, high quality, and reproducibility, producing larger parts with low-cost processes is becoming a critical threshold consideration for manufacturing the aircraft's structural components via fiber-reinforced polymer composites [6]. To this extent, the usage of autoclaves possesses numerous disadvantages, such as high capital investment and operation cost, low energy efficiency, long process times, and constraints in the part size [7]. For instance, fundamentally, this capital cost varies between approximately $200,000 for an autoclave with 1 m diameter and millions of dollars for a large autoclave [8]. Therefore, there is an obvious need for alternative manufacturing processes that replace the autoclave processes without sacrificing the part quality.

1.1 Vacuum Bag Only Prepregs

The motivation for manufacturing larger structural components at lower costs without compromising on part quality has led to the development of next-generation materials and manufacturing processes. Accordingly, the out-of-autoclave (OoA) processes have been introduced and attracted widespread acceptance over the last decade due to their abilities to deliver composites without the need for autoclaves, thereby eliminating or circumventing the limitations associated with the autoclave processes [4]. Subsequently, vacuum-bag-only (VBO) prepregs were developed specifically for OoA processes whereby high-performance primary composite

structures can be manufactured through an oven curing process at a quality level typically achievable with autoclave processes [9]. The primary advantages of VBO compared to the autoclave processing are lower capital investment, elimination of size constraints (larger parts) and the need for expensive nitrogen gas, and higher energy efficiency [10].

On the other hand, porosity and voids, which degrade the mechanical performance of the parts [3, 11, 12], are the challenging issues arisen in manufacturing composite materials; and composite parts produced with VBO processing are known to include a high amount of voids caused by trapped air bubbles. The reason for this is that, unlike the autoclave processes, the maximum consolidation pressure applied during the VBO prepreg processing is the atmospheric pressure. Considering that the fiber bed carries a fair amount of this pressure, the remaining consolidation pressure on the resin may not be sufficient to discharge or suppress voids [13]. To address this issue, VBO prepregs were designed to initially include dry and relatively permeable air channels (engineered vacuum channels or EVaCs) that allow air removal when the vacuum is applied. During the process, the resin is progressively impregnated into these channels so that it is evenly distributed and carries a low amount of voids [13]. Another striking characteristic of VBO prepregs is that they have noticeably higher resin content than conventional prepregs, and they were developed to be no-bleed systems, which means predetermined resin content specific to the application is preserved [14, 15].

Nevertheless, the physical properties of the prepreg constituents, reinforcement and matrix systems, considerably influence the evolution of VBO prepreg microstructures [16] such that changes in the properties of materials may induce significant discrepancies in resin flow rates during the cure which can lead to incomplete impregnation prior to resin gelation and microvoids in the final part. Additionally, as it was proved by several studies [16–21], resin flow dynamics and fiber impregnation in the VBO prepreg processing directly control the amount of voids contained in the final product, depending upon the removal efficacy of the trapped air within the part.

It is, therefore, critical to characterize material constitutive properties of the prepreg system to better understand migration of air bubbles, evaporated moisture, or other volatile substances towards the vacuum outlet port and impregnation behavior of the resin into dry areas prior to the gelation to produce low-void (or void-free) composite materials.

1.2 Vacuum Bag Only Prepregs Characterization

1.2.1 Resin System Properties

Thermoset type epoxy resin is commonly preferred in aerospace composite structures [3]. In its uncured state, a thermoset resin contains monomers and such additives as catalysts depending upon its formula, behaves as a highly viscous fluid. During the processing, the thermoset resin undergoes a chemical reaction, namely, polymerization induced by the catalysts. Due to crosslinking between the monomers, it evolves into a solid macromolecular structure as the monomers form long chains of polymers. As this reaction proceeds, a three-dimensional network that spans the complete material is formed due to the combination of the long polymer chains. Then, the resin undergoes a phase change and transforms into a gel/rubber in which the polymer chains prevail their mobility. In the final step, the mobility of long polymer chains is almost halted due to the completion of the crosslinking reactions, and as a result, 3d network is wholly formed. This chain of reaction, namely crosslinking, is measured by the degree of cure (α, or conversion), ranging between 0, representing the state that the resin is uncured, no-crosslinking, and 1, which means no further crosslinking can occur and the material is in its fully-cured state.

Most high-performance epoxy systems are designed to be slow-cure at room temperature to allow part preparation and treatment processes, but relatively fast at high temperatures. This curing, or crosslinking, is an exothermic reaction, and the released energy is expressed as the heat of reaction [3, 22].

The resin behavior is fundamentally influenced by the application of the temperature, namely, temperature profile during the processing of the composite material. This profile, also known as the cure cycle, is one of the process's essential parameters. Therefore, curing reaction is generally characterized through sets of dynamic scanning calorimetry (DSC) experiments following defined temperature conditions [23]. Monitoring the time history of the reaction heat can provide an accurate estimation of the resin system's curing profile.

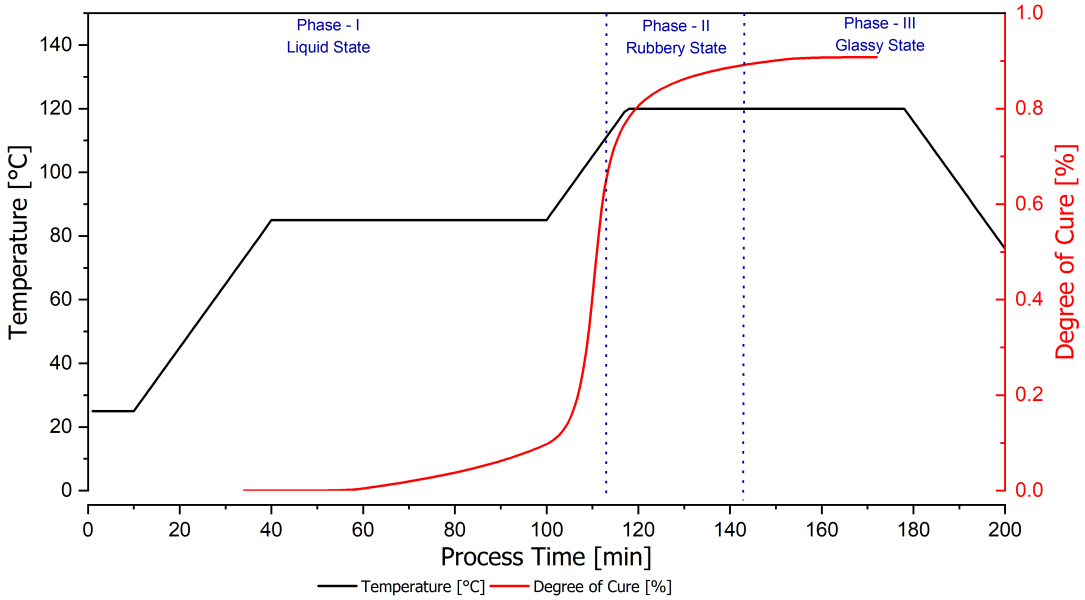

Figure 1.2 Phase changes, temperature profile and evolution of degree of cure for the OM12 epoxy resin during manufacturer's recommended cure cycle

As shown in Figure 1.2 for a typical vacuum bag only prepreg, the cure kinetics can be divided into three distinct phases depending on its behavior and chemical structure. As previously explained, the resin is highly viscous at ambient temperatures, which accounts for the beginning of Phase 1. What can be clearly seen in the figure is that the temperature increase induces the crosslinking, namely polymerization, which leads the resin to transform into a rubbery state, Phase 2. Moreover, it can be deduced that the degree of cure's progress, i.e., reaction rate, decreases as long polymer chains' mobility is restricted due to the established three-dimensional network. There is another material's property that governs its state, glass transition temperature [24, 25].

Provided that the process temperature is always higher than the glass transition temperature, the resin may preserve its rubbery state. However, this property increases in proportion to the degree of cure. Therefore, as the curing is catalyzed and accelerated during the process, the glass transition temperature eventually surpasses the processing temperature, which causes the start of Phase 3. In this phase, the mobility of the established network is highly restrained and the evolution of the degree of cure is extremely slow. At the end of the process, the highest recorded value of conversion is accepted as the ultimate degree of cure, and its temperature corresponds to the fully-cured resin's glass transition temperature [2, 26].

Upon review of the above details regarding the resin behavior during the curing, it

can be stated that the reaction rate of the curing, is principally dictated by the time and temperature inputs. Therefore, in the history of composite manufacturing processes, efforts have always been made to thoroughly understand and develop several models for the cure behavior of the resin systems, and various approaches have been put forward to clarify these relationships. Hubert et al. [22] interpreted that cure kinetics models in the literature are divided into mechanistic and semi-empirical, or phenomenological models. Mechanistic models were developed profoundly relying on the chemical composition of the resin and its molecules' interactions during the curing. Consequently, these models are harder to be established due to reaction's complexity and the undisclosed resin's chemical formula. Therefore, phenomenological models, in which the resin's chemicals are highly ignored, are favored with the aim of predicting the curing behavior specifically for the commercial thermoset resin systems. For the phenomenological models, the purpose is principally to fit an equation, including numerical constants, to an empirical data. Yousefi et al. [23] reviewed the kinetic studies of thermoset reactions and resulted that well-known cure kinetics models [27–30] were built upon the n^{th} order equations, and models originally developed by Kamal and Sourer [31], and Cole et al. [32].

On the other hand, viscosity, which defines the measure of the fluid's resistance to flow, is another critical resin property [2]. It is principally governed by the temperature and degree of cure. An increase in the temperature, and thus in the degree of cure, leads to a decrease in viscosity during Phase 1. After the curing reaction started to accelerate and the viscosity approaches its minimum value, the viscosity now increases with drastic rates due to the formation of the three-dimensional network and ultimately reaches an infinite value near the gelation point at the end of Phase 2 [26].

Hubert et al. [22] reviewed the literature and revealed that researchers focusing on the flow analysis of the composites had assumed continuously that epoxy resins obey the Newtonian behavior. This assumption was explained with several arguments such as flow through media with high fiber volume ratios is profoundly creeping and exhibit the low shear rates, and the most of the resin impregnation occurs during the phases in which the degree of cure is low [33].

The resin systems' viscosity is experimentally measured through a set of rheometer analysis under different temperature conditions, geometry types such as parallel plate, and mechanical conditions [34]. Characterization studies on the resin system's viscosity are notably correlated with other studies on the cure kinetics. Phenomenological models for the viscosity also use the same approach with the cure kinetics models and are adapted to fit an equation, including numerical parameters to the

empirical data. Common resin viscosity models [23, 29, 30] are considered to be improved versions of the Castro and Macosko's model [35].

Last but not least, the glass transition temperature (T_g) is another fundamental resin system's property that defines the point when the resin undergoes a phase change from the Phase - II towards the Phase - III as it is represented in Figure 3.5 [25]. Therefore, T_g principally governs the mechanical properties of the composite part. There are several distinct approaches to characterize the resin's glass transition temperature. The modulated DSC technique, in which the specific heat capacity of the material is used to identify the glass transition temperature; and thermo-mechanical analysis (TMA) based on the resin's thermal expansion coefficient are mostly preferred characterization methods in the literature [24, 34]. Several models available in the literature [36–40] are fundamentally based on the DiBenedetto equation to express the T_g while indicating the α as the primary input of the T_g model equation. Conversely, glass transition temperature models established upon the approaches with fitting empirical equations can also be found in the literature [34].

1.2.2 Prepreg System Properties

The reinforcement material, mostly carbon for the aerospace composite structures, have relatively higher fiber aspect ratios with diameters of almost $6-7\mu m$ and can be laid up in a configuration that it is spread over the whole part [3]. The carbon fibers are produced with different forms such as fiber tows, and weaving styles, such as unidirectional or plain, to facilitate the material preparation. Carbon fiber tows are formed such that a great number of individual fibers are bundled together. The number of fibers in a tow may vary between 3000 (3K) to 48000 (48K), and their arrangement significantly influences several important prepreg properties such as porosity and fiber volume fraction. Therefore, the morphology of the reinforcement material is considered to be an essential prepreg property. In the literature, various approaches [9, 41, 42] were adapted to characterize the prepreg systems' fiber bed morphology, and optical microscopy analysis is the widely preferred technique as it is a well-understood instrument and within easy reach in various facilities. However, sophisticated microscopy instruments such as x-ray computed tomography (micro-CT) and scanning electron microscopy (SEM) are required to further analyze the dislocations and orientations in the three-dimensional level as the capabilities that the optical microscopy offer are minimal [43].

As previously elaborated, VBO prepregs are susceptible to high void contents due to limited processing pressures up to 1 atm. In this context, the voids are one of the essential aspects of the vacuum bag only processing, and they are considered as one of the sole causes of mechanical degradations and delaminations in the final product [9, 17]. Several studies performed on the causes of void formation in composite parts manufactured with prepregs for autoclave processes and the associated mitigation mechanisms [12, 44, 45]. There are also controversies among researchers about the primary cause of voids. Some researchers claim that the moisture dissolved in resin is the primary source of voids [18], while others contend that trapped air and volatile substances are the leading cause [46, 47]. Embracing the increasing demand for the VBO process, it is essential to improve the process's success rate, which can be achieved through accurate characterization strategies, which encompasses all critical components of the VBO prepregs. However, void formation and growth mechanisms have not yet been fully understood in composite laminates produced from prepregs [17]. A systematic study of these parameters may lead to an improved justification of the void formation and growth mechanisms.

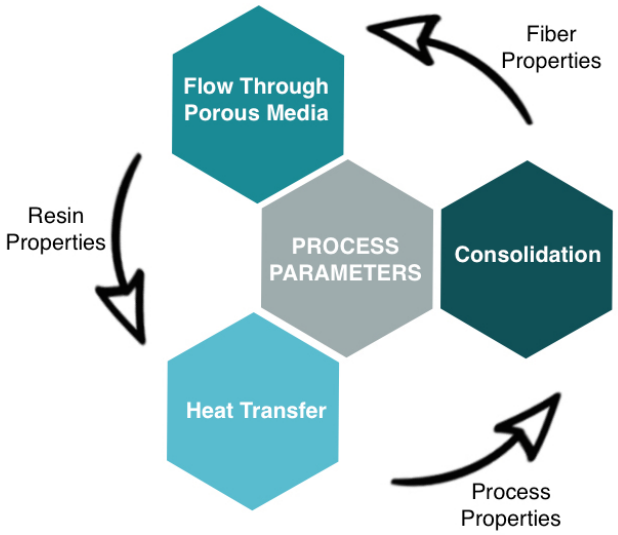

Figure 1.3 Governing physical phenomena and necessary material inputs towards the design of the process for process parameters

As in the case of many composite manufacturing techniques involving the impregnation of thermoset resins, the VBO process, in general, is governed by three separate but interdependent physics: Porous media flow, heat transfer, and consolidation mechanisms [5, 17, 20] (see Figure 1.3).

In the VBO process, flow in porous media exists due to the resin flow between fibers. Dry fibers are expected to be impregnated with the resin system while enabling the discharge of air out of prepreg to prevent void formation. Centea and Hubert [13] observed resin impregnation in various stages of the VBO process by adapting the micro-CT imaging approach. In their study, the motivation was to understand the air channels and the evacuation of the voids. Comprehensive mathematical models and experimental verifications, involving bubble migration during the resin impregnation, for the semi-impregnated prepregs are also available in the literature [19, 20, 48]. In addition to these studies, Gangloff et al. [49] evaluated void formations and bubble migration based on time, pressure, and temperature, which are among the process parameters.

Moreover, the another mechanism that needs to be included in the characterization of the prepreg material is consolidation. This step was studied in the literature with the resin flow within the fiber architecture. Various mathematical models and numerical analysis methods were developed [5, 50] to understand the effects of the consolidation mechanism on the process during the VBO processing. Gangloff et al. [48] investigated the interactions between engineered air channels and consolidation, and they demonstrated the influence of consolidation profile on void formation. In another study, Centea and Hubert [4] performed a parametric study for the consolidation profile under different pressures for the VBO process and analyzed the effect of the consolidation mechanism on the microstructure of the final product. They concluded that the effects of other process parameters need to be taken into account.

Heat transfer was included in the process by several studies in the literature based on modeling of cure kinetics and resin viscosity. The effect of cure kinetics behavior on mechanical performances and void formation, particularly in resin-rich regions, has been investigated by various studies [29–32, 51]. Hernández et al. [52] demonstrated the effects of the temperature profile applied during curing for the unidirectional (UD) prepreg system on the void volume fraction, shape, and distribution, volume and as a result, on the shear strength between layers. The most important finding of their studies is that the samples with a void volume fraction above 1% had a dramatic negative effect on inter-layer shear strength. Furthermore, cure-dependent properties of two commonly used VBO prepreg systems were characterized by Kratz et al. [30] through sets of methods described by Khoun et al [29]. In their study, the aim was to establish fundamental thermal models to develop an advanced cure cycle. They revealed that all the thermal models were highly depended upon the cure kinetics models and degree of conversion of curing profoundly governs the resin flow dynamics. They verified their arguments with experiments for the thick composite

parts. However, in the literature, the temperature values changing with the effect of cure kinetics were not included in the mathematical modeling, and the instantaneous value of the temperature during the process is not accurately characterized. This deficiency leads to inaccuracies in the viscosity, which is also depending upon the temperature.

There are also studies in the literature on the coupled effects of impregnation and cure behavior. Centea and Hubert [16] analyzed the impregnation of resin with various models including the cure kinetics and resin viscosity. They investigated effects of the fiber architecture, temperature profile during the curing, and the initial degree of cure of the resin system through parametric studies. Additionally, they incorporated several characterization studies, with the motivation of developing a model for the fiber-tow. Besides, effects of initial degree of cure on the degree of impregnation of the resin system, which changes with the out-times of the prepregs at room temperature prior to curing, were studied by neglecting other process parameters, and its effects on void formation were reported [53].

Furthermore, heat transfer of the prepreg system during the curing process is also driven by other two thermal properties; specific heat capacity and thermal conductivity. These properties have significant influence over the resin flow dynamics as the curing is dependent upon the temperature, and therefore, thermal properties of the prepreg system should also be characterized to accurately model the heat transfer throughout the prepreg system during the VBO processing and incorporate them into the integrated process model to be developed [54].

Specific heat can be expressed as the amount of heat that the material absorbs to increase the temperature as one Celsius per one gram mass and it is usually a function of temperature. DSC is one of the commonly preferred methods to measure the heat capacity of the materials [34, 55]. Since the carbon reinforced prepreg system consists of reinforcement and the resin materials, specific heat capacity of each composition should be investigated individually in order to realistically characterize the thermal behavior of the prepreg system. In the literature, specific heat capacity was considered as a single input to the models and its evolution during the curing was not thorougly characterized [30, 54, 55]. Kalogiannakis et al. [56] investigated specific heat capacity behavior of the carbon/epoxy and glass/epoxy cross-ply laminates with a Modulated Temperature Differential Scanning Calorimetry (MTDSC). They revealed that heat capacity was almost doubled between pre- and post-glass transition stages, and therefore, the heat capacity of the composites is strongly dependent on the temperature.

On the other hand, thermal conductivity has also a fundamental role during the

VBO processes as it influences the heat dissipation of the material. It is one of the transport properties of the material with regards to the heat conduction which is calculated in terms of Fourier's Law. Materials with high thermal conductivity can transfer the heat with a higher heat rate than the materials with low thermal conductivity. Furthermore, inhomogeneous materials like fiber reinforced composites result in anisotropic thermal conductivity along the different fiber orientations. For instance, a carbon fiber reinforced prepreg material with unidirectional fiber orientation does have different thermal conductivities in different directions as it is illustrated below in Figure 1.4.

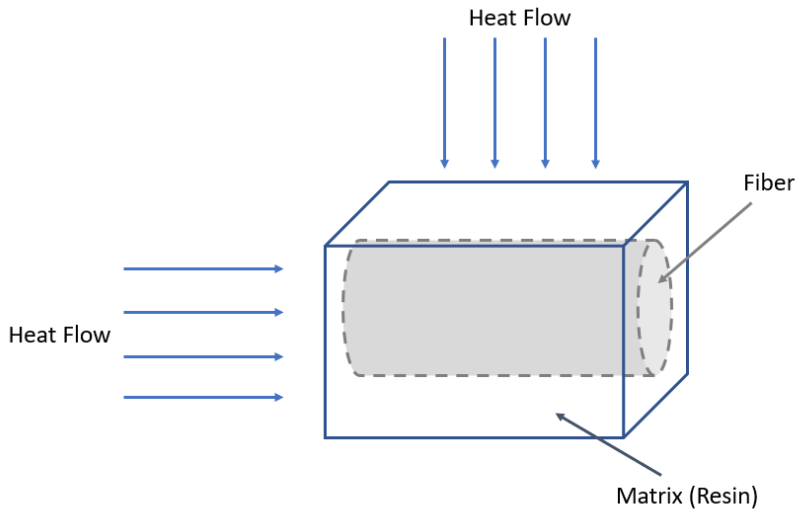

Figure 1.4 Anisotropic thermal conductivity of a composite system with a unidirectional fiber orientation

As can be interpreted from the above explanations, thermal conductivity of a composite material depends on the fiber/resin distribution and fiber orientation. This statement can be exemplified as follows; a carbon fiber reinforced composite material with a unidirectional fiber orientation demonstrate different thermal conductivities in the in-plane and through-thickness directions as it is illustrated in Figure 1.5.

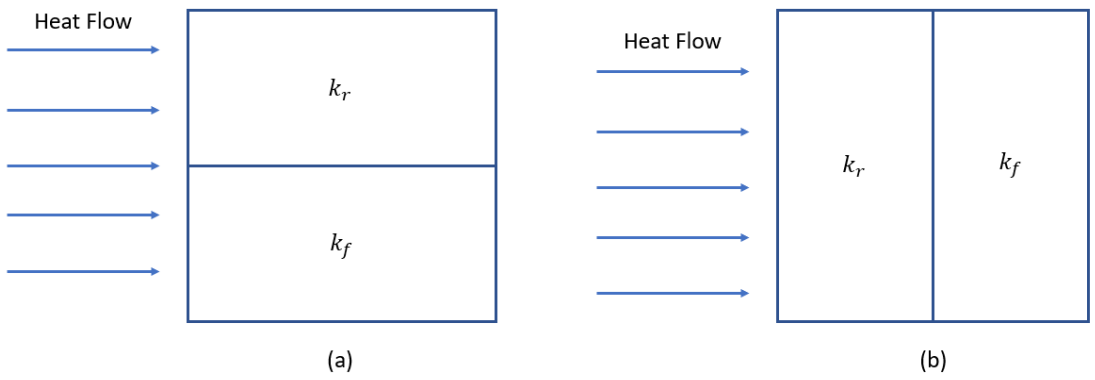

Figure 1.5 Anisotropic thermal conductivities for the heat flow (a) along the fiber direction $k_{\parallel}$; (b) transverse to the fiber direction $k_{\perp}$

In Figure 1.5, k_f and k_r are the thermal conductivities of the fiber and resin, respectively. Here, illustrated heat flows passing through this composite system along the different directions (parallel and perpendicular to the fiber orientation) results in different thermal gradients as a result of anisotropic composition and geometrical orientation of the composite.

1.3 Thesis Objectives and Structure

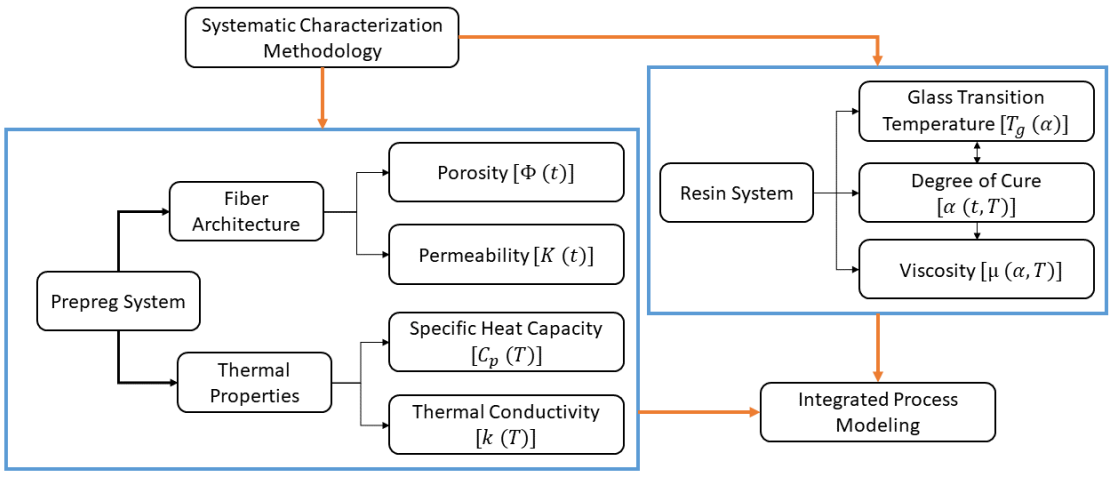

Figure 1.6 Systematic characterization methodology for the VBO prepreg system

Considering the studies that take the VBO prepregs from various perspectives, to the best of authors' knowledge, there is no characterization study in the literature,

which focuses on all of the relevant material properties and the process mechanisms altogether for the VBO prepregs as presented in Figure 1.6. For this reason, there is a vital need for a systematic and overarching characterization methodology. The present study intends to establish a methodology that systematically characterizes such factors as material properties and constitutive behavior to strengthen the VBO prepreg process model's accuracy and reliability. To achieve this goal, this approach was applied to characterize a commercial VBO prepreg system's properties and processing parameters. Hence, the present thesis is organized into the following chapters:

Chapter 2: Cure-dependent properties of the resin system were characterized regarding cure kinetics, rheology, and glass transition temperature by semi-empirical phenomenological models.

Chapter 3: The first fiber architecture, void-content change, the fiber volume fraction of the prepreg system were investigated through sets of x-ray tomography scans of the laminates processed to different stages of curing. The initial permeability behavior of the porous media was modeled through a CFD analysis of the selected domain. Finally, the specific heat capacity and thermal conductivity of the constituents' thermal properties were investigated by a series of experiments.

Chapter 4: The conclusions of this research are drawn and future works that can further expand the knowledge obtained during this study.

2. RESIN SYSTEM CHARACTERIZATION

The present chapter focuses on understanding the resin system behavior of the material throughout the cure cycle by providing the details of each step with the motivation of leading the way to designing a cure cycle.

The main properties of resin system are divided into three types of parameters: (1) degree of cure [α], (2) viscosity [μ], and (3) glass transition temperature [T_g] to develop an integrated process-based model for the epoxy resin. These properties are interdependent based on one parameter, α. The following sections will present the material properties and characterization methodology of resin system's primary properties. The experimental procedure and numerical models and the results will be evaluated in detail.

2.1 Materials

The reference material for this study was KOM12/KCF12KUD300 carbon fiber reinforced prepreg developed by the KORDSA for the Vacuum Bag Only (VBO) processes. The prepreg system contains 40% resin content by weight and the reinforcement weave is unidirectional with the tow size of 12K (means that 12000 carbon fibers per tow) and carbon fiber weight ratio of $300 g/m^2$. Furthermore, this prepreg system has the following densities of the constituents as $1800 kg/m^3$ for the resin and $1850 kg/m^3$ for the reinforcement material. The thermoset type resin system, OM12, was developed for this prepreg and formulated for an initial cure at 80–130℃ and Table 2.1 summarizes the recommended cure conditions. This resin system has not been extensively investigated, and therefore, the parameters to be adopted in the resin system behavior models require to be determined. The materials were subjected to experiments under 12 hours of being removed from storage in the freezer kept below -18℃ to preserve similar out-time conditions between samples.

Table 2.1 OM12 resin system recommended cure conditions

Property	Oven/Vacuum bag	
Typical Ramp Rate	1 – 2 °C/min	
Cure Temperature	80 °C	120 °C
Cure Dwell Time	12 hours	1 hour
Cure Pressure	-1 bar	
Dry Tg (DMA)	<100 °C	>110 °C

2.2 Cure Kinetics

Cure cycles are developed to satisfy several performance measures for the thermosetting composites. Cure kinetics model which is one of the fundamental considerations for the cure cycles, gains a significance to obtain the high-performance end-products [5]. There are many developed models to accurately characterize the resin cure kinetics through the performed experiments and mathematical models in the literature [29–32]. The degree of cure and cure rate of the resin system can be determined through a set of dynamic scanning calorimeter (DSC) tests in dynamic and isothermal conditions and phenomenological models which can provide significant contribution regarding the design of cure cycles without the need for experimental steps [30]. The developed methodology of cure kinetics characterization in this study is interpreted in Figure 2.1.

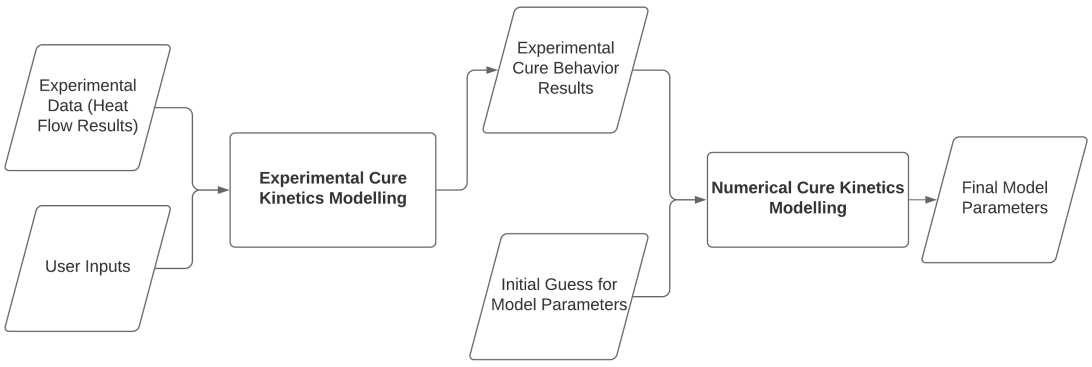

Figure 2.1 Schematic of the cure kinetics model parameters prediction scheme

The following subsections will explain the cure kinetics characterization for an epoxy

resin system with regards to experimental procedure, the predicted cure kinetics model and results.

2.2.1 Experimental Work

The heat flow data obtained from Dynamic Scanning Calorimeter (DSC) experiments is required to understand the degree of cure and cure rate behavior of the resin system. The neat resin system's heat flow was measured through sets of experiments performed under dynamic and isothermal conditions using A Mettler Toledo DSC 3+ (see Figure 2.2). This DSC equipment measures the released (or absorbed) heat of the reaction by either heating/cooling or keeping constant the temperature of the furnace chamber which the sample is placed in. The operation procedure of the equipment is as follows. Measurement cell placed in a completely sealed furnace chamber and the cell includes 2 pans. The first pan is for the reference and the resin is put into the second pan, and both pans are placed on the same heater via an autosampler. The predetermined experiment method and conditions are automatically applied to the furnace chamber to ensure that both pans are subjected to the same experiment environment. The only difference is that one pan includes the predetermined amount of resin, therefore, it requires to be exposed to more heat to keep the heating rate uniformly for the both pans. Thus, DSC equipment generates the heat flow data by thermocouples placed below the measurement cells through the temperature values for the cells (reference and sample cells) and the corresponding temperature.

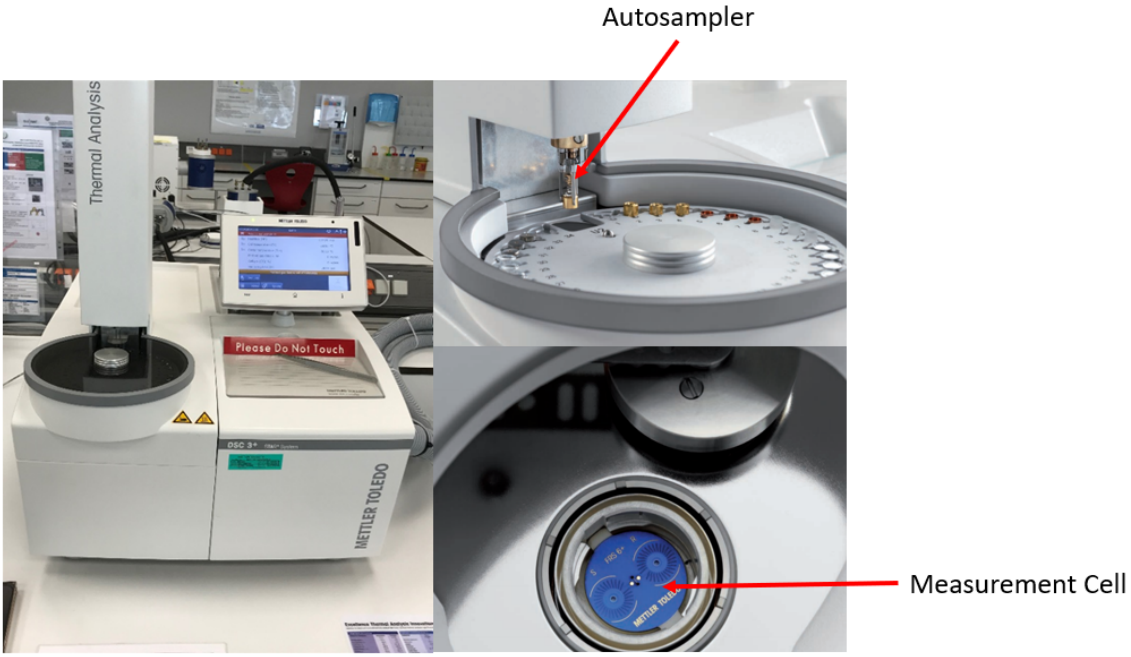

Figure 2.2 DSC testing equipment (left), sample holder (right-top), measurement cell (right-bottom)

To prepare the test specimens, the epoxy resin was removed from the freezer where it is stored at -18°C and kept at room temperature. The mass of samples varied between 6-16 mg, and the samples were placed in aluminum pans sealed by a press unit. Then, the samples in sealed pans were placed in their corresponding positions by the autosampler.

There were four performed sets of dynamic scans starting from -60°C up to 350°C to determine the resin system's total heat reaction. Furthermore, three different temperatures were selected to perform the isothermal runs with the motivation of determining the isothermal heat of the resin. After each isotherm is completed, the sample is cooled to the (23°C) room temperature and heated up with a predetermined heating rate up to 300 °C to determine the residual heat of the reaction. Each experiment was carried out up to two times in order to validate reproducibility of the results. Below predetermined dynamic and isothermal conditions are summarized in Table 2.2.

Table 2.2 OM12 Resin System Cure Kinetics Test Matrix

Condition	Temperature (°C)	Time (min)	Heating Rate (°C/min)	Residual Temperature (°C)	No. Tests
Dynamic	350		5		2
	350		10		2
	350		15		2
	350		20		2
Isothermal	100	120	10	300	2
	120	60	10	300	2
	150	60	10	300	2

2.2.2 Cure Kinetics Modeling

As previously stated, cure kinetics model is fundamental to design the cure cycles for the thermosetting composites. Cure kinetics model is simply the relation which expresses cure rate of the reaction as a function of degree of cure.

A variety of cure kinetics models were developed with the goal of predicting the epoxy resin systems' cure behavior numerically. They can be divided into two categories as mechanistic and phenomenological models. Mechanistic models are built upon the understanding reaction occurs between the chemical models during the cure process. However, this form of reactions are highly complex and mechanistic models for that reason mechanistic models are considerably difficult to be established. Therefore, phenomenological models have been developed to model the resin system's curing behavior to eliminate the need for the details of the chemical reaction [29]. Hence, the phenomenological models are commonly preferred to model cure behavior of the thermoset resins. Phenomenological cure kinetics models are obtained through several DSC experiments conducted in dynamic/isothermal conditions.

In this study, a semi empirical mathematical model is developed as described by Khoun et al. [29] to accurately characterize the cure kinetics of the resin system and accordingly to predict the degree of cure which demonstrates the extent of the chemical reaction.

A program is developed in MATLAB environment and consists of two different part: Experimental cure kinetics modelling and numerical cure kinetics modelling.

The user inputs the experimental data, heat flow results of the experiments, with other properties such as sample mass, total heat of reaction, etc. and the program explicitly calculates the experimental degree of cure and cure rate. The second program carries out a minimization procedure to identify the necessary parameters that the model can predict the degree of cure behavior with the smallest residual. A least squares nonlinear regression method approach was utilized to determine the required numerical parameters of the cure kinetics model. This program can perform on multiple curves (sets of experimental data) simultaneously and results in one set of parameters that are applicable for all the cases.

This mathematical model predicts the degree of cure behavior of the resin system through any time-temperature history. After all the experiments are completed, the first step is to convert the heat flow values obtained from dynamic runs to the reaction's total heat. This can be simply described as the area between the heat flow and the baseline curves as demonstrated in Figure 2.3. The average total heat of reaction for the OM12 resin system was determined as 340 J/g with a standard deviation of 3%.

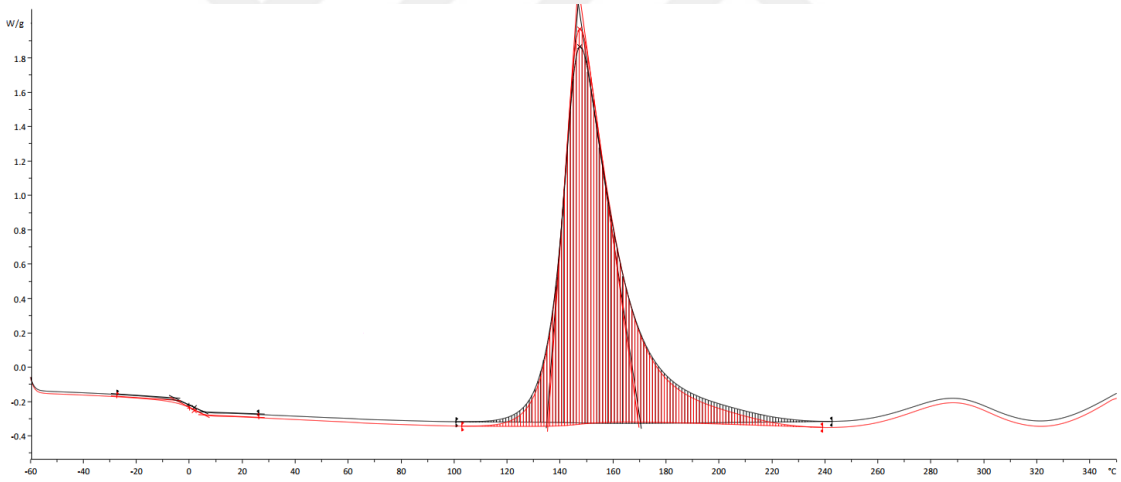

Figure 2.3 Heat flow versus temperature data obtained from two DSC dynamic scans at 10 ℃/min from -60 ℃ up to 350 ℃ with an integral tangential baseline curve

On the other hand, the degree of cure (α) is determined through the isothermal scans by comparing the isothermal (H_I) and residual (H_R) heats of the reaction with a fixed total (H_T) heat of the reaction as it is stated in Equation 2.1.

$$\alpha = \frac{H_T - H_R}{H_T} \tag{2.1}$$

Degree of cure behavior of the resin system for different conditions could be obtained with Equation 2.1 and then it was utilized to set the baseline to find out the isotherm

values as in Equation 2.2 which contributes to determine the experimental cure rate ($d\alpha/dt$) of the reactions provided in the Equation 2.3.

$$H_I + H_R = H_T \tag{2.2}$$

$$\frac{d\alpha}{dt} = \frac{1}{H_T}\frac{dH}{dt} \tag{2.3}$$

Many efforts have been made to predict the resin's degree of cure, and the most widely used models were based upon the Kamal & Sourour's cure model [31]:

$$\frac{d\alpha}{dt} = (K_1 + K_2\alpha^m)(1-\alpha)^n \tag{2.4}$$

In this equation, K_1 and K_2 are the reaction rates and they are described by the Arrhenius temperature dependency equation, below. Additionally m and n correspond to the reaction orders.

$$K_i = A_i e^{\frac{-E_{A_i}}{RT}}, i = 1, 2 \tag{2.5}$$

This model (Equation 2.4) incorporates and merge two different cure models, namely n^{th} order and auto-catalytic models. However, these models were distinctively generated based on the chemical reaction mechanisms of the resin system. Arguing that the effect of these models should be taken into consideration separately, Lee et al. [28] introduced an improved version (Equation 2.6) of Kamal & Sourour's model to effectively break down the equation into two parts to distinguish the chemical mechanisms' effects.

$$\frac{d\alpha}{dt} = K_1(1-\alpha)^{n_1} + K_2\alpha^m(1-\alpha)^{n_2} \tag{2.6}$$

These models were the fundamental tools toward a successful prediction study for the resin system's degree of cure behavior. However, as previously explained in the Introduction chapter, once the curing is accelerated and the T_g surpasses the cure temperature, the resin undergoes a phase change. The established network's mobility is highly constrained, and the degree of cure is prolonged due to the diffusion effect. Additionally, most common thermoset resin types do not reach a fully-cured state at temperatures below 180°C due to the same effect. Therefore, Hubert et al. [27] proposed a diffusion-controlled autocatalytic-type cure model (Equation 2.7), which was an extended version of Lee's model. This equation calculates the degree of conversion as a function, primarily governed by the time and temperature parame-

ters. Experimental values were used to fit the parameters to this diffusion-controlled autocatalytic equation:

$$\frac{d\alpha}{dt} = K_1\alpha^{m_1}(1-\alpha)^{n1} + \frac{K_2\alpha^{m_2}(1-\alpha)^{n2}}{1+e^{D(\alpha-(\alpha_{C0}+\alpha_{CT}T)))}} \tag{2.7}$$

Table 2.3 lists the parameters and their definitions included in the cure model equations.

Table 2.3 Cure kinetics model parameters and their definitions

Model Parameter	Definition
A_i	Pre-exponential coefficients
E_{A_i}	Activation energies
R	Universal gas constant
T	Absolute temperature
D	Diffusion constant
m_1, m_2, n_1, n_2	Model constants
α_{C0}	Critical α at 0 K
α_{CT}	Increase in α with temperature

E_A is obtained from the Arrhenius equation provided below

$$\frac{d\alpha}{dt} = Ae^{\frac{E_A}{RT}} \tag{2.8}$$

which can be rewritten as:

$$\ln(\frac{d\alpha}{dt}) = \ln(A) - \frac{E_A}{RT} \tag{2.9}$$

As recommended by Khoun et al. [29], a point where the degree of cure lower than 0.1 was selected to calculate the E_A through the equations 2.8 and 2.9 and the slope of $\ln(d\alpha/dt)$ versus $1/T$. This procedure was repeated for the other activation energy value. Additionally, a linear relationship could be achieved between the α_{max} and T_g. Hence, α_{C0} and α_{CT} were determined as equation parameters of the linear fit, as shown in Figure 2.5. The other parameters, A_1, A_2, m_1, m_2, n_1, n_2 were determined by applying a least squares nonlinear regression between the $d\alpha/dt$ and the α values for the complete set of experimental conditions.

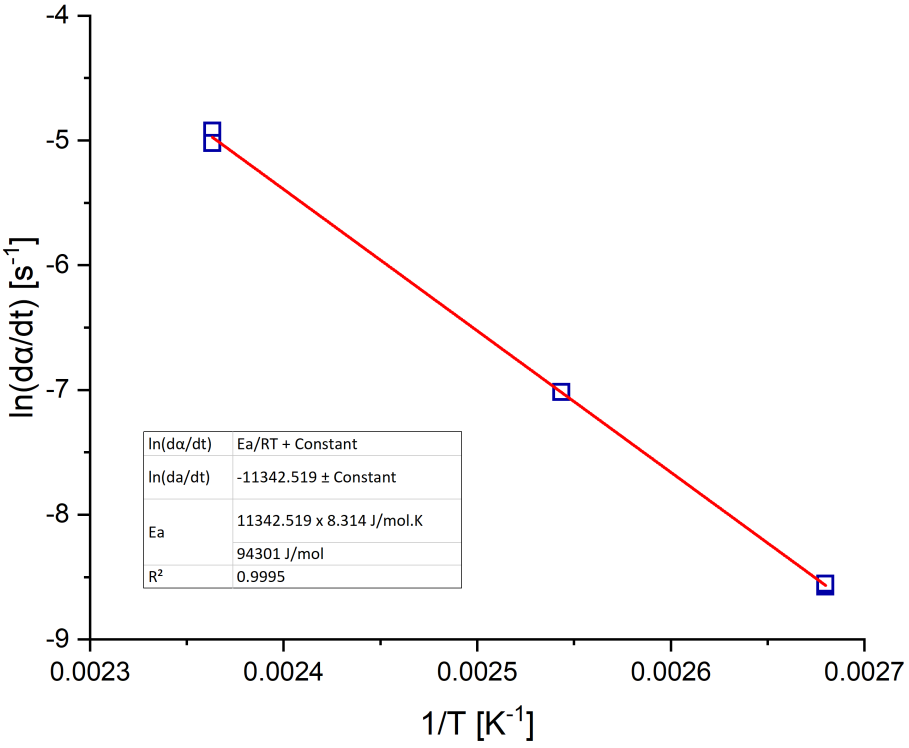

Figure 2.4 Natural logarithm of the $d\alpha/dt$ as a function of $1/T$ at a low conversion value ($\alpha = 0.1$) under isothermal conditions

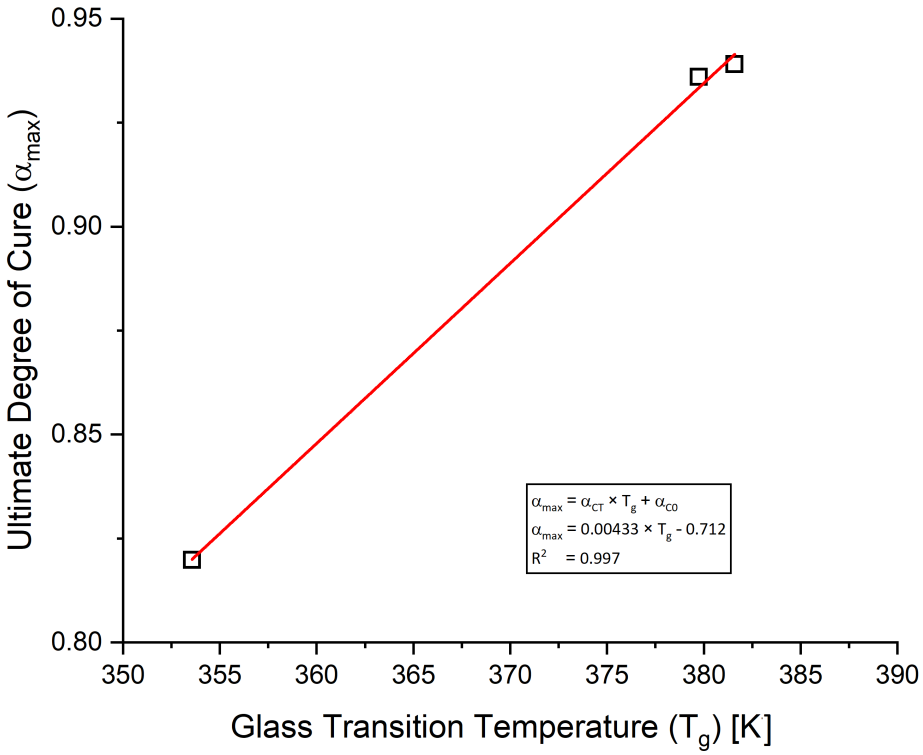

Figure 2.5 α_{max} under isothermal conditions as a function of T_g

2.2.3 Modeling Results and Discussion

Several efforts were made to determine the principal equation for the cure kinetics model among the previously explained models (Equation 2.4, 2.6 and 2.7). Hubert's diffusion-controlled autocatalytic model (Equation 2.7) was preferred in this study along with the parameters listed in Table 2.3. The reason why this model was taken as a reference for the fitting step was that it delivered the most successful fitting results for the thermoset resin system used in this study. One fundamental characteristic of this model was to have an additional numerical constant, which allowed the author to manipulate the code more unobstructedly and thus successfully.

All the dynamic and isothermal trials were fitted simultaneously, and one certain set of parameters could be obtained which are applicable for all the cases. The final parameters for the cure kinetics model are listed in Table 2.4. Figure 2.6 represents the degree of cure evolution of the resin system under dynamic and isothermal conditions along with the model predictions. Overall, the cure kinetics model accu-

rately predicts the curing evolution of resin system for both dynamic and isothermal conditions. The model slightly deviates from the experimental degree of cure for isothermal dwells at 120 and 150℃ . However, this imperfection can be tolerated as the success of the fit is indicated by the R^2 values above 0.96.

Table 2.4 OM12 Resin System Cure Kinetics Model Parameters

Final Parameters	Value
Heat of Reaction	340 J/g
Pre-exponential cure rate coefficient of reaction I (A_1)	$1.41 \times 10^5\ s^{-1}$
Activation energy of reaction I (E_1)	$66.190 \times 10^3\ J/mol$
Pre-exponential cure rate coefficient of reaction II (A_2)	$1.32 \times 10^2 s^{-1}$
Activation energy of reaction II (E_2)	$89.505 \times 10^3\ J/mol$
1st exponential constant (m_1)	0.708
2nd exponential constant (m_2)	0.901
3rd exponential constant (n_1)	1.754
4th exponential constant (n_2)	0.5
Diffusion Constant (D)	88.97
Critical α at 0 K (α_{C0})	$-$ 0.6685
Increase in α with temperature (α_{CT})	$7 \times 10^{-4}\ K^{-1}$

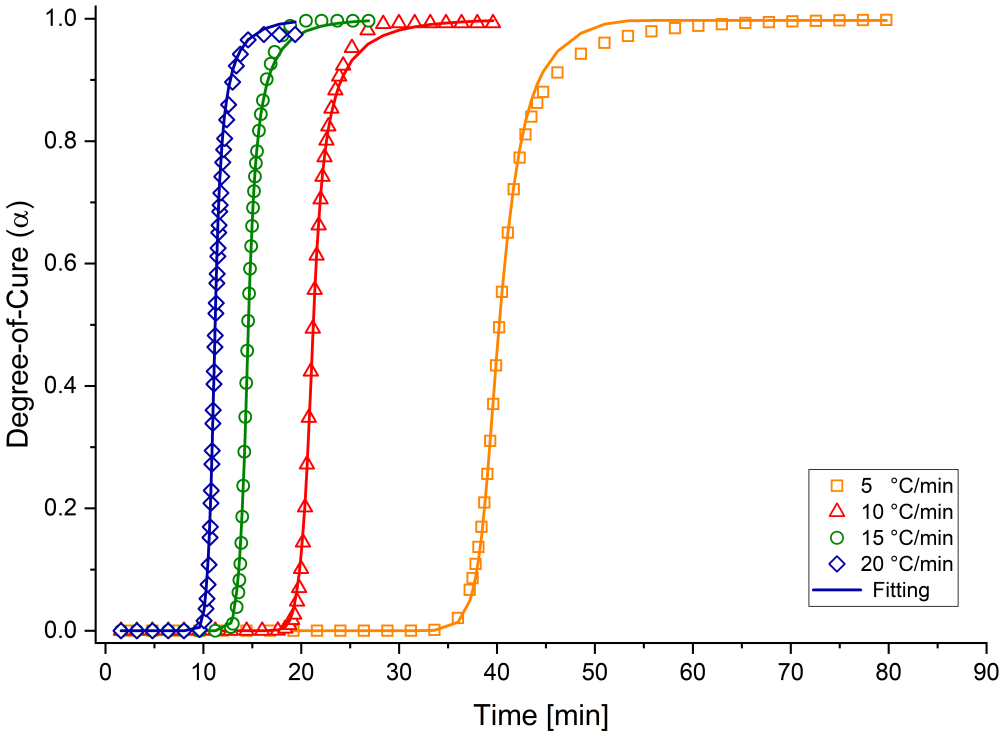

(a)

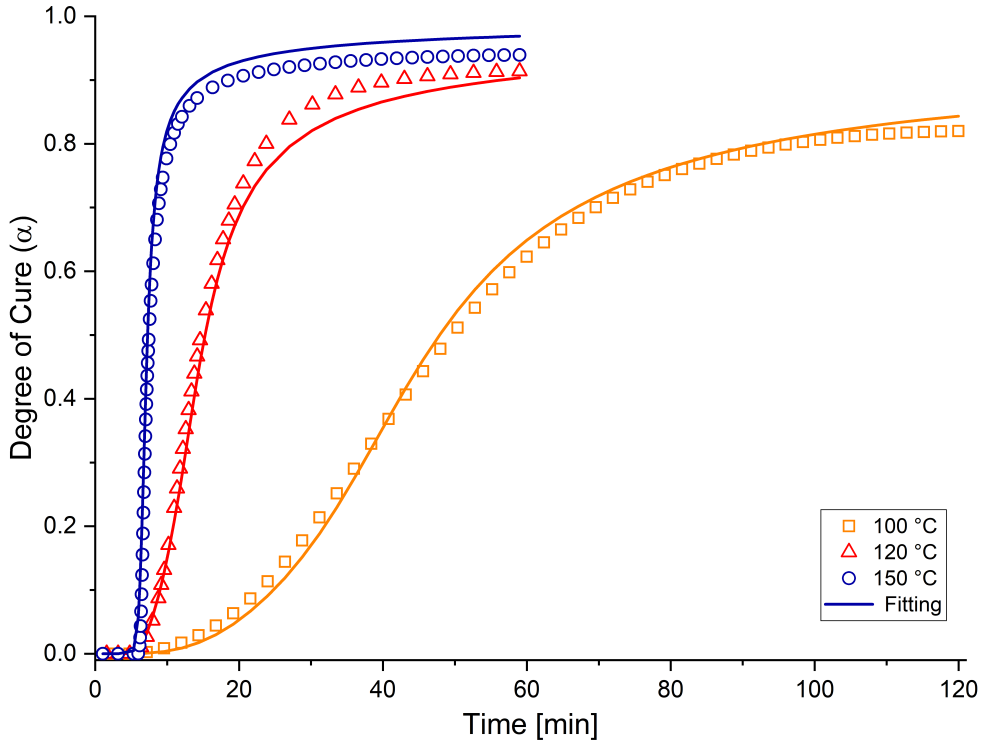

(b)

Figure 2.6 The evolution of the degree of cure during the cure cycle of (a) dynamic and (b) isothermal trials. The experimental data (symbols) is compared with the model predictions (continuous lines)

2.3 Viscosity

Understanding the rheological behavior of the resin system is fundamental as the viscosity is one of the important parameters to figure out and control the void content of the composite parts during the process [30]. Furthermore, the viscosity is controlled by two parameters: temperature ramp rate which identifies the corresponding temperature of the minimum achieved viscosity and the dwell temperature which governs the period of time that the resin can flow into dry regions of the fibre as the resin is in liquid form.

In the literature, several models were proposed to characterize the resin system's rheology through the performed experiments and mathematical models in the literature [29, 30]. The resin system's viscosity can be characterized through these semi-empirical models, incorporating temperature- and degree of cure-dependent equations by coupling with cure kinetics model elaborated in the previous section. Through these models, viscosity, degree of cure and gelation point of the resin can be predicted for any temperature cycle without the need for experimental steps. The developed methodology of rheology characterization in this study is interpreted in Figure 2.7.

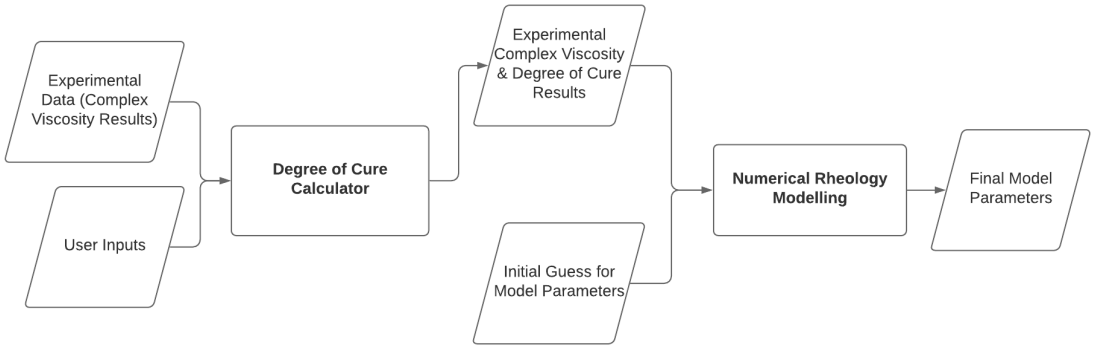

Figure 2.7 Schematic of the rheological model parameters prediction scheme

Following subsections describe the rheological characterization of epoxy resin systems with regards to experimental procedure, adapted numerical model and results of the study.

2.3.1 Experimental Work and Results

The rheological behavior of the neat resin was characterized by using an Anton Paar MCR 702 TwinDrive rheometer. This advanced instrument encloses an Environmental Test Chamber (ETC) to regulate the specimen's temperature. Figure 2.8 depicts the rheometer and detailed view for the ETC and highlighting the neat resin between $25mm$ disposable parallel plates.

Figure 2.8 Rheometer (left); environmental test chamber (ETC) detailed view (right-top); close-up view of the Disposable parallel plates and the resin specimen (right-bottom) [57]

There are 4 performed sets of dynamic scans starting from 50°C up to 160°C with a variety of temperature ramps between 1-4°C/min and 4 sets of isothermal dwells between 100-140°C. The complete test matrix for the rheology characterization of the OM12 resin system is provided below in Table 2.5.

Table 2.5 OM12 resin system rheology characterization test matrix

Condition	Temperature (°C)	Heating Rate (°C/min)	No. Tests
Dynamic		1	2
		2	2
		3	2
		4	2
Isothermal	110	20	2
	120	20	2
	130	20	2
	140	20	2

The experiments conducted at a controlled strain of 0.01% and a constant frequency of 1 Hz until the termination criteria, $Loss\ Modulus = Storage\ Modulus\ and\ tan(\delta) = 1\ (G - crossoverpoint)$, was reached. To prepare the test specimens, the epoxy resin was removed from the freezer where it is stored at -18°C and kept at room temperature. The resin specimens were placed between disposable parallel plates with a diameter of $25mm$ and the thickness of $1mm$ and the disposable parallel plate attachment was connected to the draw rod. Then, the environmental test chamber (ETC) closed to seal the experiment environment and the medium was heated to 50°C prior to perform the experiment.

The dynamic and isothermal viscosity behavior of the resin system is exhibited in Figure 2.9. According to the dynamic tests, until the point where the resin viscosity reached a minimum value, the increase in the temperature leads to a decrease in the viscosity. Additionally, the ramp rate does not have a role in the change in viscosity of the resin system viscosity until 100°C. With the start of the curing reaction, the viscosity value rapidly increases, thereby eliminating the decreasing effect of temperature on viscosity. Isothermal tests demonstrate that the required amount of time in which the resin is still liquid and can flow into dry regions until the gelation point where the viscosity abruptly increases in a short period. Additionally, the resin system did not reach the gelation point during the 2-hour long isothermal dwell at 80°C. This behavior can prove that an isothermal hold at 80°C before the final dwell temperature yields more extra time for the fluid resin to impregnate into dry fabric areas.

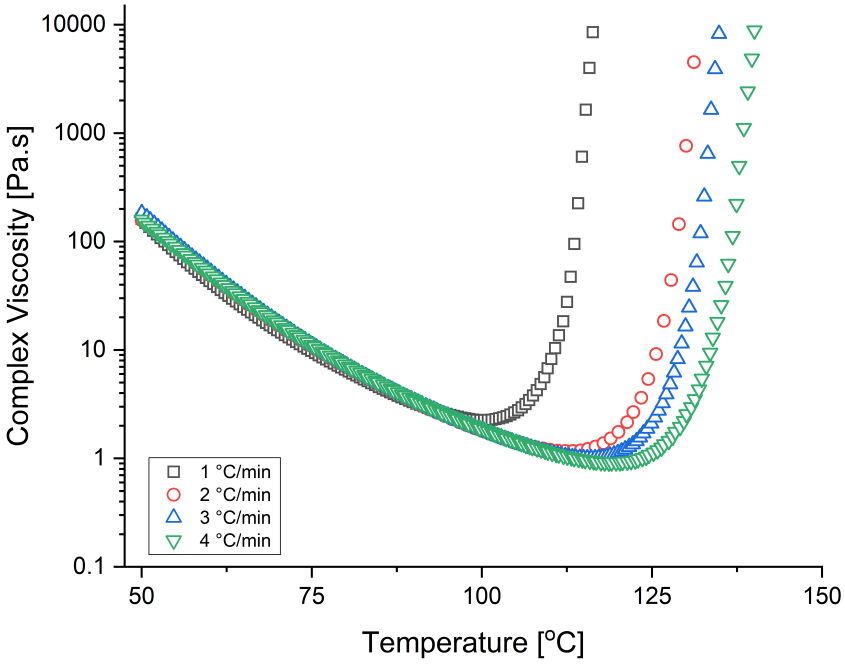

(a)

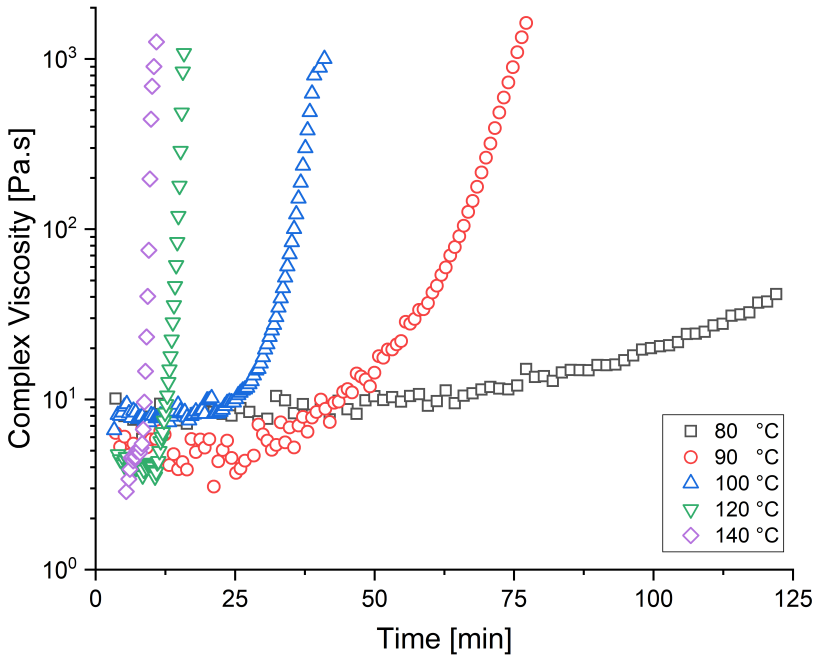

(b)

Figure 2.9 (a) Dynamic and (b) isothermal viscosity behavior of the OM12 resin system

2.3.2 Resin Viscosity Modeling

The resin system's viscosity can be predicted at any point and any temperature cycle as a function of T and α through the developed semi-empirical models coupled with the cure kinetics model. The viscosity model used in this study was proposed by Khoun et al. [29]. They adopted a model, which includes the effects of gelation, formerly established by Castro et al. [35]. This model incorporates extra parameters, second Arrhenius temperature dependency and a polynomial term to the exponential terms, to clarify the resin's viscosity behavior. The model equation is as follows:

$$\mu = \mu_1 + \mu_2 \left(\frac{\alpha_{gel}}{\alpha_{gel} - \alpha} \right)^{A + B\alpha + C\alpha^2} \tag{2.10}$$

$$\mu_i = A_{\mu_i} e^{\frac{E_{\mu_i}}{RT}} \ , \ i = 1, 2 \tag{2.11}$$

Table 2.6 lists the parameters and their definitions included in the viscosity model equations.

Table 2.6 Viscosity model parameters and their definitions

Model Parameter	Definition
A_{μ_i}	Pre-exponential coefficients
$E_{A_{\mu}i}$	Activation energies
R	Universal gas constant
T	Absolute temperature
A, B, C	Model constants
α_{gel}	α value at gelation point

The viscosity activation energy E_{μ_i} and A_{μ_i} were determined following the same approach explained in the cure kinetics section. The $\ln(\mu)$ against $1/T$ were plotted from room temperature until a point where viscosity exhibited an increase. The slope and intercept of the linear trendline were used to determine E_{μ} and A_{μ}, respectively.

Additionally, degree of cure at gelation point, α_{gel}, was determined to be 0.75 by taking the average of G-cross over point $Loss\ Modulus = Storage\ Modulus\ and\ tan(\delta) = 1\ (G - crossoverpoint)$ from the each dynamic and isothermal experiment.

A program is developed in MATLAB environment and consists of two different part:

Degree of cure calculation and numerical viscosity modelling. The user inputs the experimental data obtained through the rheometer to the first part. Then, the program explicitly predicts the degree of cure behavior of the resin system during the rheology experiments based on the cure kinetics characterization methodology described in the previous section which incorporates the equations 2.7 & 2.5 along with the predetermined parameters provided in Table 2.4. The second part of the program carries out a minimization procedure to identify the necessary parameters that the model can predict the viscosity behavior with the smallest residual. A least squares nonlinear regression method approach was utilized to determine the required numerical parameters of the viscosity model. This program can perform on multiple curves (sets of experimental data) simultaneously and results in one set of parameters that are applicable for all the cases.

2.3.3 Modeling Results and Discussion

In this study, experiments performed under isothermal conditions were ignored since those data exhibited notable deviations over the predefined isothermal dwell temperature. This might result from inconsistency between the resin type, such as fast cure or slow cure, and the inputted parameters such as frequency and strain.

All the dynamic trials were fitted simultaneously and one set of parameters were obtained for the OM12 resin system viscosity model (see Table 2.7). Figure 2.10 represents the measured viscosity response of the resin system under a set of dynamic conditions along with the model predictions. Overall, the model exhibits a good agreement with the experimental data and correctly predicts the onset of gelation of the resin system and is valid until the gelation point, which is $\alpha = 0.75$ for OM12 resin system.

There is a slight deviation between the experimental and predicted viscosity values; the model underestimated the minimum viscosity value and viscosity at the gelation point for 1°C/min temperature ramp. On the other hand, the viscosity model successfully captured the evolution of the resin viscosity, temperature ramp, and gelation for temperatures ramp greater than 1°C/min. Additionally, considering the fact that the OM12 resin system is developed for cure temperatures between 80-130°C, this model will precisely predict the viscosity evolution during the temperature ramp.

Table 2.7 OM12 Resin System Rheology Model Parameters

Final Parameter	Value
Pre-exponential viscosity coefficient I (A_{μ_1})	$2.49 \times 10^{-19}\ s^{-1}$
Activation energy of reaction I (E_{μ_1})	$91 \times 10^{3}\ J/mol$
Pre-exponential viscosity coefficient II (A_{μ_2})	$3.4 \times 10^{-8}\ s^{-1}$
Activation energy of reaction II (E_{μ_2})	$46 \times 10^{3}\ J/mol$
1st exponential constant (A)	10
2nd exponential constant (B)	-15
3rd exponential constant (C)	1.3
Degree of cure at gel point (α_{gel})	0.75

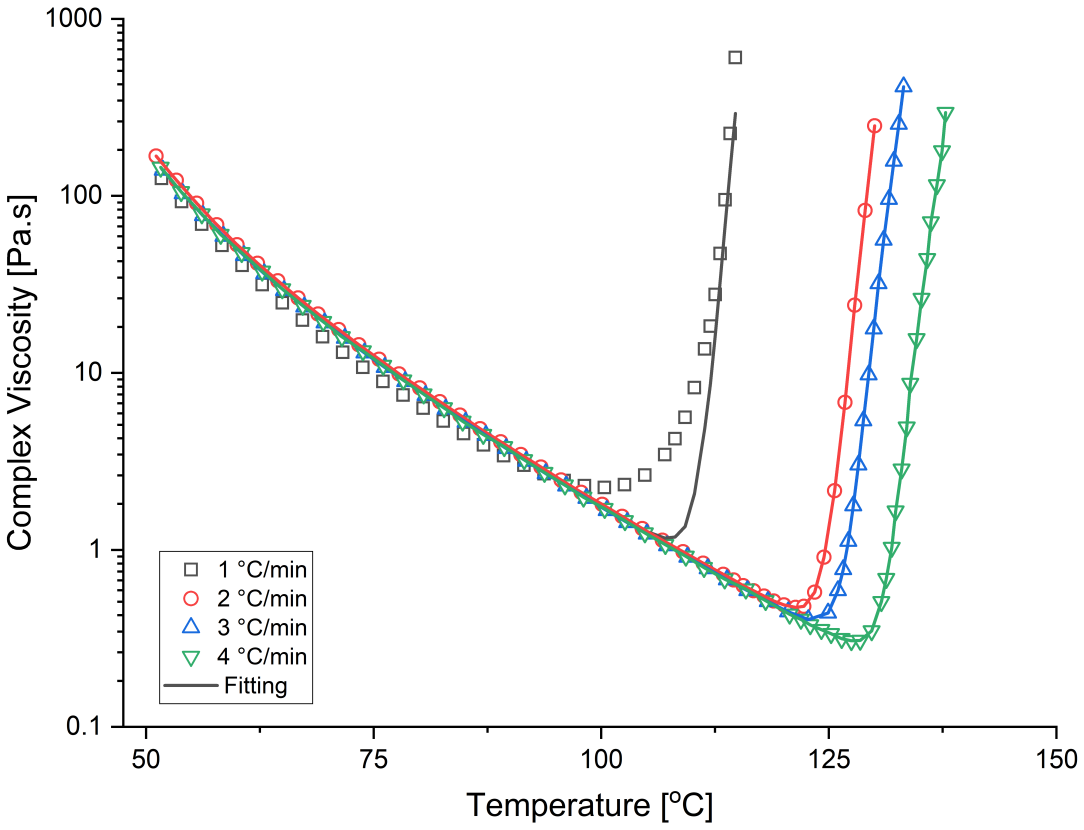

Figure 2.10 The evolution of the complex viscosity during the experiments in dynamic conditions. The experimental data (symbols) is compared with the model predictions (continuous lines).

2.4 Glass Transition Temperature (T_g)

T_g is a significant material property that determines the uppermost processing temperature of a polymeric material. The polymer is in a hard-glassy state before the T_g, and after the T_g point is surpassed, the polymer trends towards a rubbery state. The most common methods utilize DSC, in which a step-change in specific heat capacity of the material predicts the T_g; dynamic mechanical analysis (DMA), which periodically applies a mechanical force to the specimen while the temperature of the chamber is increased.

2.4.1 Experimental Work and Results

In this study, DSC method was preferred to identify the Tg of the partially cured resin samples. As explained in the cure kinetics modeling section, after each isothermal dwell, samples were cooled down to the room temperature and heated up with a certain temperature rate up to 300°C T_g of the partially cured resin was taken as the midpoint in the dramatic change in the heat flow versus temperature graph during the ramp. This procedure was repeated twice for all isothermal DSC experiments, and the average T_g values are presented in Figure 2.11.

The highest recorded T_g was identified as the fully-cured resin system's glass transition temperature, and this value was validated with a DMA analysis performed with the fully-cured prepreg samples. For this analysis, eight plies of prepreg were laminated and subjected to curing in a conventional oven following the manufacturer's recommended cure cycle. After curing, samples were subjected to tests in a three-point bending mode of a Mettler Toledo DMA/SDTA 861e dynamic mechanical analyzer. $100mm$ sinusoidal displacements were applied to the samples at a frequency of 1 Hz, while they were heated-up 3°C/min.

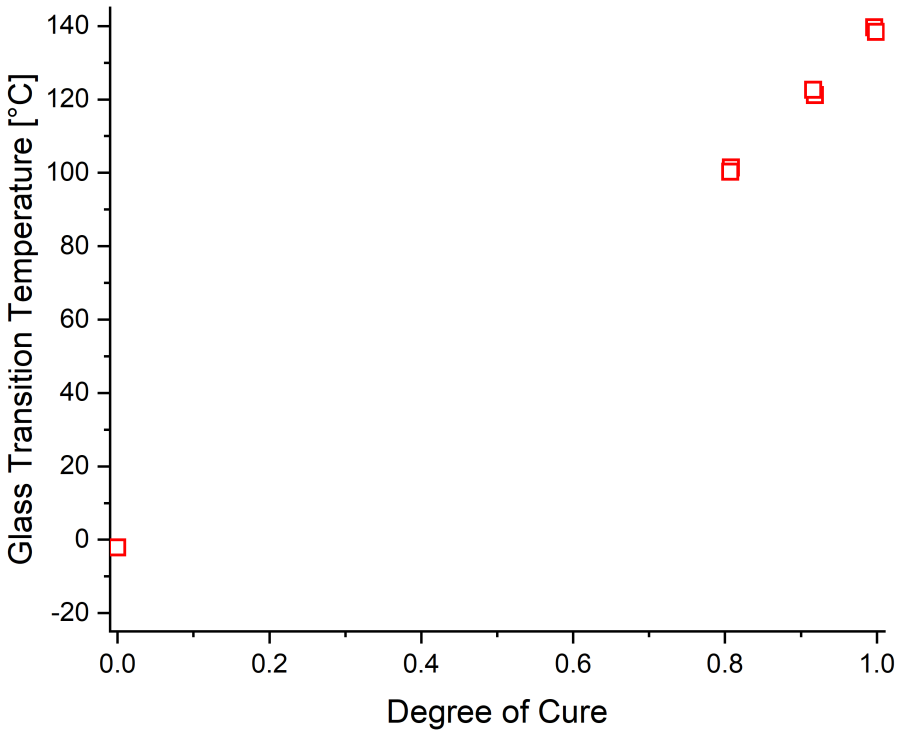

Figure 2.11 Evolution of the midpoint of the glass transition temperature.

2.4.2 T_g Modeling

T_g of the neat resin was modeled using the residual part of the isothermal DSC scans and fitting the DiBenedetto [58] model equation the experimental data. In the DiBenedetto equation Equation 2.12, T_g was fundamentally governed by the α. λ is a fitting parameter in this equation and predicted based on the least-squares nonlinear regression.

$$\frac{T_g - T_{g0}}{T_{g\infty} - T_{g0}} = \frac{\lambda\alpha}{1-(1-\lambda)\alpha} \tag{2.12}$$

Table 2.8 lists the parameters and their definitions included in the T_g model equations.

Table 2.8 T_g model parameters and their definitions

Model Parameter	Definition
T_{g0}	T_g of the uncured resin
(T_{g_∞})	T_g of the fully-cured resin
λ	Fitting parameter

2.4.3 Modeling Results and Discussion

The fitting results of the T_g model are compared with the experimental T_g values in Figure 2.12. It was demonstrated that the T_g model accurately predicts the resin system's glass transition temperature behavior. Equation 2.12, along with the parameters listed in Table 2.9, can predict the evolution of T_g of the resin system at any degree of cure history.

Table 2.9 Glass transition temperature model parameters

Final Parameter	Value
T_{g0}	-1.69°C
$T_{g\infty}$	139.54°C
λ	0.6221

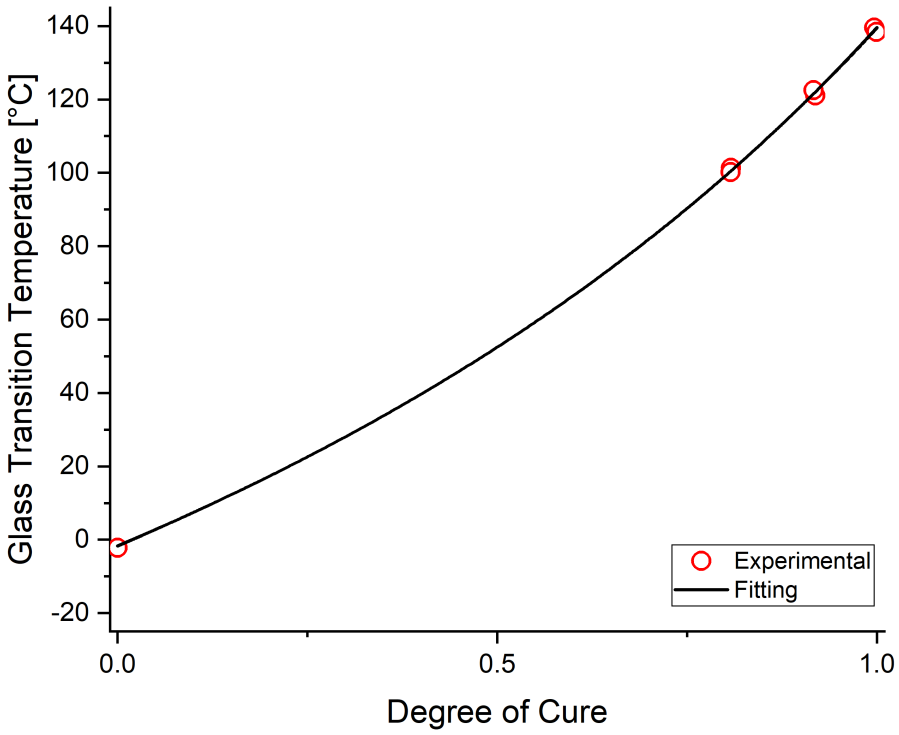

Figure 2.12 The measured and predicted glass transition temperature for OM12 resin system

2.5 Summary

In this chapter, a systematic methodology used to characterize the constitutive material properties of the OM12 resin system was presented. This involved various sets of experiments using DSC, rheometer, and DMA apparatus to fit the semi-empirical models to the experimental data. A diffusion-controlled cure kinetics model was found to precisely predict the resin's cure behavior at any time-temperature history. The cure kinetics model was used to adapt a viscosity and glass transition temperature models. The viscosity model successfully predicted the evolution of resin rheological behavior and the onset of the gelation point. Finally, the glass transition temperature was used to determine the upper operating temperature of the resin system.

Although the parameter identification characterization models may seem very

straightforward, several complications have appeared that make it more difficult. Particular attention should be paid to the storage and shell-time of, specifically, a fast-cure resin system before testing. The analysis process reveals its complications with baseline selection. Finally, there are many approaches in the fitting process, and each possesses different challenges. In this case, although some parameters are not as expected, moderate accuracies can be obtained for different sets of experimental data. Ultimately, it was revealed that the presented methodology yields the results that are consistent with experimental data. However, different models are required to be investigated for such-fast curing resin systems.

With the models presented in this chapter, an integrated out-of-autoclave process model incorporating thermoset resin can be successfully established, and an appropriate cure cycle can be designed for the composites manufactured with an OM12 resin system.

3. PREPREG SYSTEM CHARACTERIZATION

Dry fiber fabrics should be successfully impregnated with the resin in the resin film regions by air evacuation during the consolidation and subsequent oven curing stage based upon the requirements of VBO processes. Since the leading concern is the resin flow into dry fabric regions, it is essential to comprehend the first fiber architecture and porosity along with the permeability behavior of the reinforcement system. Additionally, such thermal properties as specific heat capacity and thermal conductivity of the prepreg constituents possess significant influence over the resin flow dynamics as the curing is dependent upon the temperature, and therefore, thermal properties of the resin system should also be characterized.

3.1 Reinforcement System

3.1.1 Tow Modeling

The prepreg used in this study has unidirectionally placed fiber bundles (tows), each comprises of 12000 (12K) fibers with a specific elliptical shape. To define reasonable dimensions for the tow geometry, several prepreg plies were examined with a light microscope, and an average tow size was obtained.

3.1.1.1 Experimental Work

Uncured composite prepreg samples were used for the examination of the macro structures of the samples. For this, KOM12 prepreg samples were removed from the freezer where they were kept at -18°C and kept for a while at room temperature. Then, the prepreg samples cut into four similar parts by means of a pair of scissors from different locations of the prepreg fabric were placed between the aluminum layers in transparent epoxy resin molds and the resins were left to dry at room temperature.

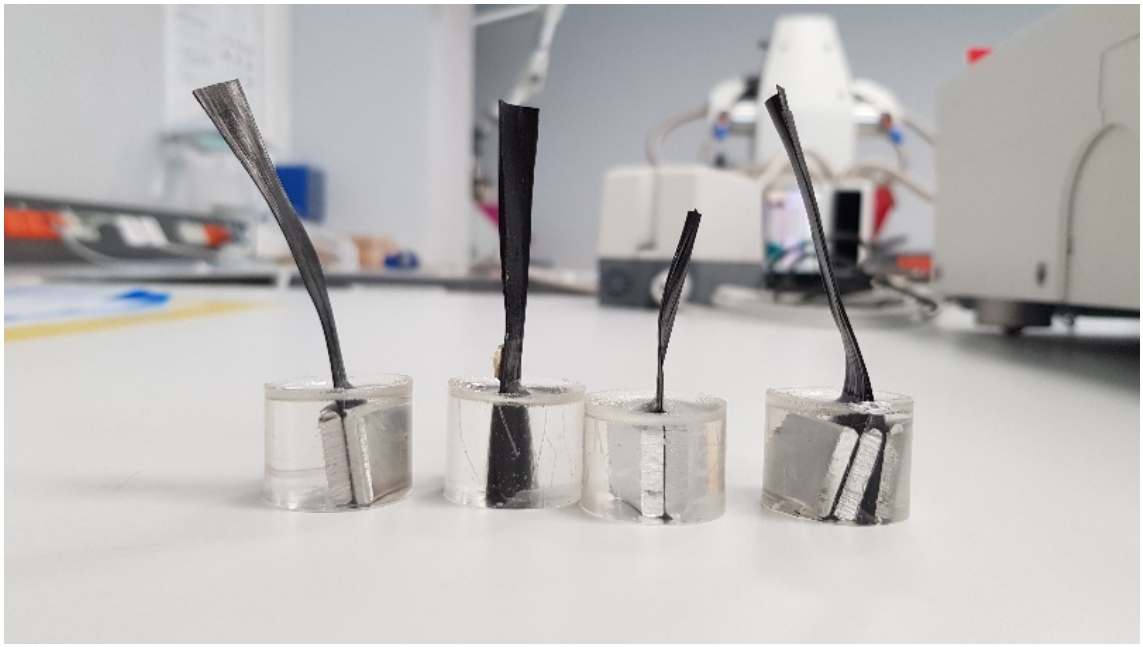

Figure 3.1 Prepreg samples placed between aluminum sheets in transparent epoxy

Figure 3.1 shows the prepreg samples contained in the dried transparent epoxy resins. Prepreg samples were subjected to sanding and polishing along the axis perpendicular to the fiber bundles by cutting off the excess portions, respectively. LaboForce 100 sanding and polishing device developed by Struers was used for these processes. Sanding and polishing processes were carried out by following the steps in Table 3.1 and Table 3.2 below. Also, Struers brand DiaDuo 2 water-based suspensions were preferred for polishing.

Table 3.1 Sanding process steps

Process Type	Consumable Type	Amount of Meshes in Consumable	Amount of Applied Force (N)	Rotational Speed (rpm)	Process Time (min)
Sanding	Silicon Carbide	300	10	100	1
		500	20	150	3
		1000	20	150	6
		2400	20	150	3

Table 3.2 Polishing process steps

Process Type	Consumable Type	Abrasive & Particle Size	Amount of Applied Force (N)	Rotational Speed (rpm)	Process Time (min)
Polishing	MD-Dur	Diamond & 1 µm	30	150	5

The primary purpose of the embedding prepreg samples into the epoxy resin and subjecting them to sanding and polishing processes was to eliminate the prepreg layer exposed to the shear force due to the scissor's effect used to separate the prepreg laminates into pieces, and thus, accurately analyze the fiber-tows and resin fractions and orientations in the inner regions that were not exposed to shear force.

Following the polishing process, Nikon Eclipse LV100ND optical microscope was used to examine fiber bundles and resin orientation. This study, where prepreg samples were analyzed throughout the thickness (see Figure 3.2), aimed to obtain representative fiber and resin distributions and fiber bundle geometric dimensions.

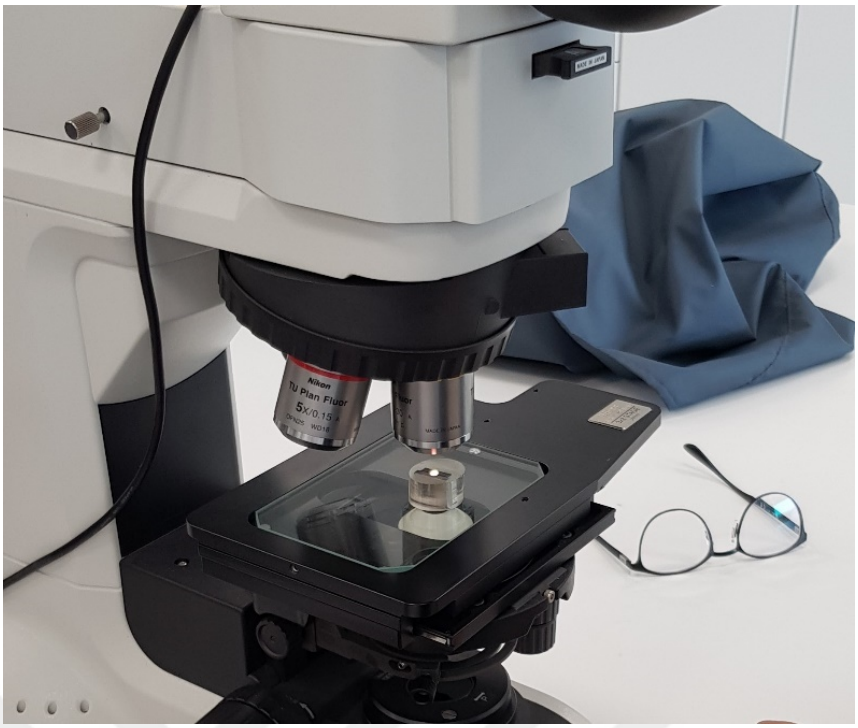

Figure 3.2 Optical microscope setup to analyze cross-sectional fiber/resin orientation (50-times zoomed to the sample)

3.1.1.2 Results

Figure 3.3 presents the cross-sectional view of a prepreg ply with average tow dimensions, representative fiber-tows orientation and resin distribution referenced as a result of this study. In the figure, the prepreg sample appears between two layers of aluminum (the lower and upper bright pieces). Dark regions scattered through the prepreg or concentrated in particular regions represent dry fiber tow areas not impregnated by the resin. The lighter gray areas indicate dense areas in terms of resin. Besides, the dark region with elliptical shape in the center of the sample corresponds to a fiber-tow.

Furthermore, average diameter of the individual carbon fibers were found to be 6 μm which is an essential first step towards the establishing model domain for the permeability characterization.

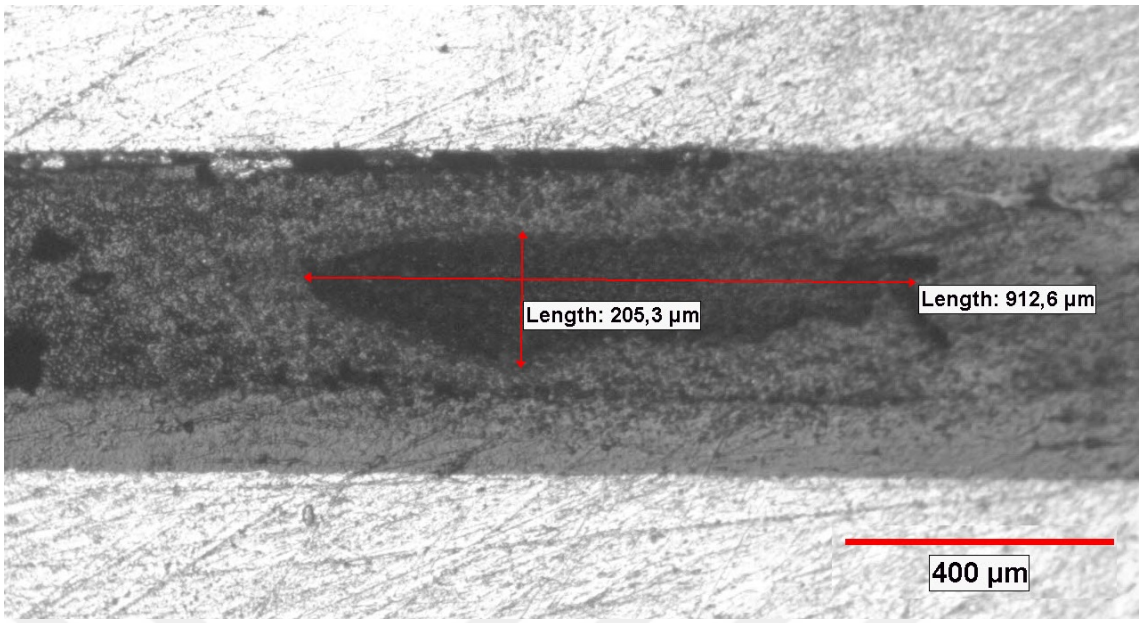

Figure 3.3 The cross-sectional view of the referenced prepreg ply highlighting the average dimensions of a tow

3.1.2 Porosity Analysis

3.1.2.1 Preparation and Processing

To understand the pre- and post-process properties of the reinforcement system, a list of processed laminates are prepared for the subsequent scanning operations, and these laminates can be grouped as uncured and cured as summarized in Table 3.3.

Table 3.3 List and characteristics of processed laminates

Laminates	A	B	C	D
Process Condition	Uncured		Cured	
Number of Layers	1	2	1	2

Thirty centimeters by 30cm laminates were prepared for the two uncured laminate processing scenarios. First, the samples (A and B) were cut from the center of each of the laminates with the dimensions $10x10mm$. A set of laminates proceeded to the scanning step, whereas another set (consisting of 2 plies) was compacted through

the application of a force on top/bottom layers.

As for the cured laminates scenario, $30x30cm$ laminates are prepared for the oven-curing process. One set of laminate had one-ply while another set of laminate consisted of 2 plies, each was laid-up by laying the prepreg plies on a flat aluminum tool plate. A perforated release film was laid on top of the prepreg stacks to enable the air-evacuation through-thickness. Edge breather plies are placed between and top of the prepreg plies to create an open pore network to uphold the connectivity between the vacuum port and the resin-free cross-sections of the fabric in each lamina plane. A layer of breather cloth blanketed the whole arrangement. An inlet and outlet vacuum valve system and the vacuum bag closed the lay-up (see Figure 3.4). The process cycle for the laminates started with a 10-minutes vacuum hold at 25°C, 2°C/min ramp to 85°C for an hour-long isothermal dwell, and another ramp to 120°C (final cure temperature) for another an hour-long isothermal dwell followed by cooling with 2°C/min ramp to 60°C for a total process time of 210 mins. Once the cooling step completed, the laminates were removed from the oven and relieved from the vacuum source. The skin temperature of the laminates was tracked using thermocouples during the entire process cycle.

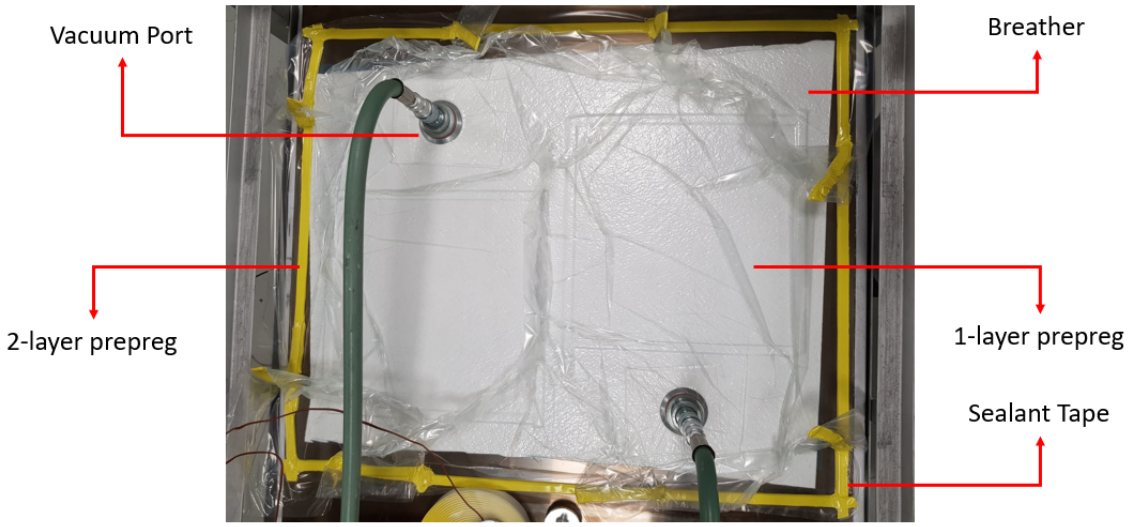

Figure 3.4 The vacuum bag arrangement of the processed laminates

Following the curing process, two samples (C and D) with the dimensions of $10x10mm$ were cut from the center of the two cured laminates.

3.1.2.2 Micro-CT Analysis

In this study, Skyscan's 1172 High-Resolution Micro-CT was used as the tomography system of the scanning operations. Relevant scanning parameters (see Table 3.4) were adjusted with the motivation of acquiring the optimum contrast between carbon fiber, epoxy resin, and the voids, and by taking Centea and Hubert's [13] proposed scan parameters. The resolution of the scan is expressed as the size of the smallest detail (pixel) that is scanned. The highest attainable resolution was the $1.75\mu m/pixel$ value determined for sample A to have a detailed scan output for the resin/fiber locations. However, it should be noted that the output scan possessed a great deal of noise and relatively small sample size (4 mm per side maximum) due to high capture resolution. Therefore, the $3\mu m/pixel$ value was determined for samples B, C, and D to scan a reasonable sample size (10 mm per side maximum) while maintaining an acceptable contrast between the constituents. On the other hand, as for the image size, which can be described as the number of pixels in the field of view of the detector, the maximum available value of 4000 x 2096 $pixels$ was preferred for all the scans.

Table 3.4 Micro-CT scanning parameters

Parameter	Value
Filter	None
X-ray voltage	62 kV
X-ray intensity	$161\mu A$
Resolution	$1.75 - 3\mu m/pixel$
Image size	4000 x 2096 $pixels$

The prepreg sample can be mounted on a sample holder in two different configurations: embedding in a foam block with a cut hole or holding in place with an adhesive putty on top of the holder. Both configurations were identical regarding the quality of the scan, but the latter was preferred to avoid the possible distortion. Micro-CT took approximately two hours for each sample for 360° rotation.

The tomography system delivers the scans as raw shadow projections, and (Skyscan) Nrecon software was utilized to reconstruct the projections into sequences of parallel X-ray micrographs. Reconstruction settings as misalignment compensation, ring artifact reduction, and beam hardening reduction were adjusted for each set of micrographs through a series of performed parametric studies with NRecon's fine-tuning option. Each sample required approximately two hours of reconstruction times.

3.1.2.3 Void Content Analysis

The change in the macro-void content at each stage was quantified using Skyscan's CTAn, 3d image analysis software. First, reconstructed CT images were separated into solids (reinforcement and matrix system) and voids applying a grayscale threshold. Then, the thresholded (binary) images, comprises of both white (solid) and black (void) pixels, were subjected to a series of algorithms (Despeckle, Bitwise operations) and morphological operations to eliminate the noise and micro-voids introduced by X-ray imaging, and obtain the best region of interest for each micro-slice of the processed files. Finally, the resultant CT images were analyzed by the "3D Analysis" plug-in to obtain the void content of the processed images enclosed by the region of interest.

Furthermore, a slice present at the center of the image sequence was selected to determine the average ply thickness of each sample, and it was calculated by measuring the thickness of the sample and dividing by the number of layers.

3.1.2.4 Fiber Volume Fraction

The evolution of fiber volume fraction was calculated by using ImageJ, an open-source image analysis software. The reconstructed CT images were imported into the software and were thresholded with a higher grayscale value to separate the raw images into black (reinforcement) and white (resin and voids). Then, a series of the region of interests manually selected from the first, intermediate, and end slices to interpolate them for the optimum region of interest per micro-slice. Following, a 2d analysis was performed to measure the area fraction of the fibers inside the region of interest for each slice, and the resultant set of fractions was averaged to obtain the fiber volume fraction of the sample.

Additionally, the initial fiber volume fraction was validated through a molecular weight analysis. According the standardized test methods (like ASTM C613 - 19) to investigate the volume fractions of the constituents of the composite materials, the matrix (resin) should be physically removed by either dissolving or burning off to avoid the chemical effects on the reinforcement material (fiber) for the calculation of the resin/fiber fractions with regards to weight or volume. Due to the distinctive chemical properties of the prepreg samples, the dissolving method was preferred. A VELP Scientifica automatic solvent extractor (SER 158 Series) was used to re-

move the matrix material from the carbon fiber reinforcement by dissolving. This experiment was performed three times to obtain more realistic values.

The mass of the sample and the crucible were independently measured and noted as the initial mass (M_i) and (M_c), respectively. Then, the sample was placed in the crucible of test equipment and the test was initialized to dissolve the resin out of the prepreg material. The mass of the sample remained in the crucible after the test was measured and noted as final mass $\left(M_f\right)$ after applying the below equation.

$$M_f = M_{crucible+fiber} - M_{crucible} \tag{3.1}$$

Hence, the mass of the reinforcement material and weight fractions of the constituent materials can be easily calculated as provided below:

$$m_r = \frac{M_i - M_f}{M_i} \tag{3.2}$$

where m_r represents the weight fraction of the resin system. It is already known that $\rho_{fiber} = 1850\ kg/m^3$ and $\rho_{resin} = 1180\ kg/m^3$. By applying the rule of mixtures and knowing the densities of resin and reinforcement, the initial fiber volume fraction was calculated to be 31.4%. Table 3.5 summarizes the calculated weight and volume fractions of the constituents.

Table 3.5 Weight and volume fractions of the matrix and reinforcement material

	Matrix Material		Reinforcement Material	
	m_r	v_r	m_f	v_f
Mean Values	0.4044	0.343	0.5956	0.314

3.1.2.5 Results and Discussions

Micro-CT Analysis

The applied cure cycle temperature, the predicted degree of cure, and viscosity properties of the resin system were calculated by the Equations 2.7 and 2.10. The predicted resin degree of cure could reach up to $\alpha = 0.9$. In contrast, the predicted

resin viscosity decreased from almost $\mu = 1600Pa.s$ (at room temperature) to a minimum value of $\mu = 10Pa.s$ (at the beginning of the 85℃ isotherm) throughout the cure cycle. During the first dwell (at 85℃), the viscosity gradually increased, however, with the crystallization kinetics of the resin system, the viscosity ascended very quickly to the gelation point (predicted to be $\alpha = 0.75$) despite the contrary effect of the temperature ramp on the viscosity.

In Figure 3.5, voids are denoted as black since these areas possess zero attenuation. In contrast, brighter grayscale values stand for denser, resin-rich regions.

Sample A depicts the very first state, uncompacted and uncured, of a prepreg ply in detail. Resin films are placed on top/bottom of the ply and denoted with relatively brighter grayscale value, and one can assume that these resin films do not contain fibers. On the other hand, fiber bed is present between the resin films and depicted with the brightest grayscale value. Furthermore, a mixture of solids and black voids, as magnified with additional box, represents the dry fiber tow areas and resin-rich regions surrounding these areas. Additionally, large gaps are present within the dry fibre regions due to entrapped air between dry fiber tows in the preparation process. Sample B presents a compacted and uncured laminate consisting of two prepreg plies. In this case, the laminate possesses fewer inter-ply voids as a result of compaction, and local larger gaps are present, possibly because of the wrinkling during the compaction. Although dry fiber tow regions are now smaller, they still remain moderately dry as they are not fully infiltrated with the resin. It should also be noted that the scan resolution for sample A is almost twice better than for sample B, but with a relatively smaller scanned area. Therefore, it is harder to distinguish the resin-rich or dry fiber tow areas as the fronts have slightly vanished in the Sample B micrograph. However, tow boundaries or fiber accumulations can be detected with a detailed inspection, as it is highlighted in the magnified insertion.

Samples C and D represent consolidated and cured prepreg laminates. Both samples were obtained with the manufacturer's recommended curing cycle (MRCC) under the same ambient conditions and have the equivalent scanning parameters with the Sample A. As can be seen from the insertion boxes, Sample C stands out as a prepreg in which a large proportion of local voids were eliminated. Similar comments can be made for Sample D, two-layer prepreg. In sample D that was subjected to consolidation and curing processes, macro-sized voids were eliminated, and inter-layer voids and wrinkle marks were mostly removed. However, in Sample D, the resin can be distinguished as thin strip layers at the top and bottom, although it largely penetrated into and around the dry fiber tow areas. The reason for this can be expressed that the process parameters, optimum for a single layer of prepreg,

could not demonstrate sufficient success for the two-layered prepreg, and the resin could not infuse to the inter-layer regions prior to the completion of curing reaction.

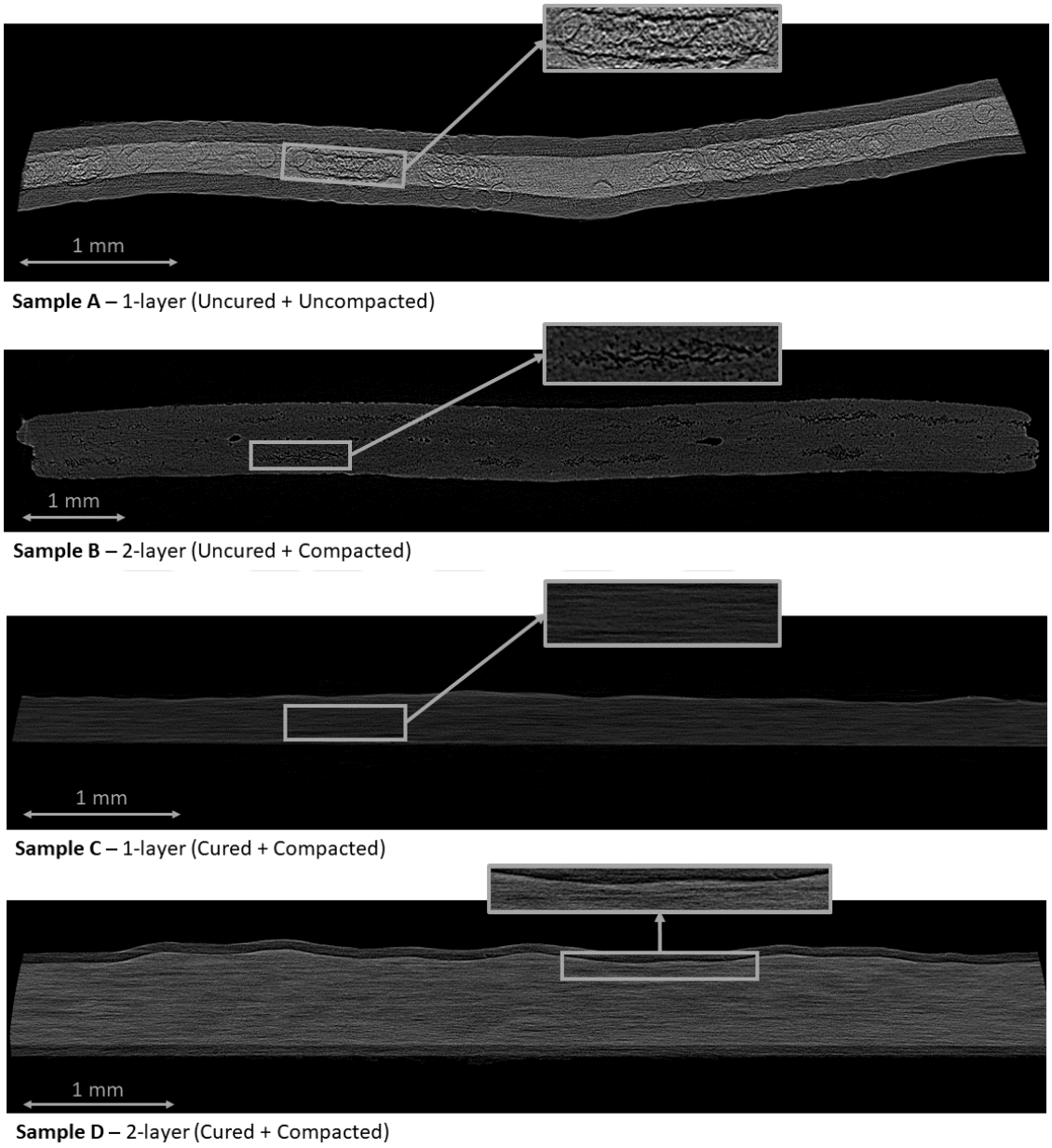

Figure 3.5 X-ray micrographs (samples A-B-C-D). The additional inserts highlight; the visible dry fiber tow areas for samples A and B; relatively dry regions for samples C and D.

Void Content and Fiber Volume Fraction Measurements

The measured data are presented in Table 3.6 along with their corresponding process stage. As expected, the uncured and uncompacted sample exhibits higher void content percentage and average ply thickness, and lower fiber volume fraction. Subsequent to the application of consolidation and curing, void content percentage, and average ply thickness demonstrate a noticeable decrease, while the fiber volume frac-

tion increases to a large extent. This highlights the significance of the application of consolidation after each lay-up on the purpose of closing the inter-ply gaps and leading the remaining air to the EVaCs during the processing. Evidently, a significant increase in fiber volume fractions could be observed as a result of consolidation and curing processes for the single layer prepreg samples (A and C). However, the reason that there is less increase in the fiber volume fractions of two-layer prepregs (samples B and D) compared to other samples (A and C) can be explained that sample B scanned prior to curing was already subjected to a consolidation application. In addition, as previously stated, the consolidated and cured single layer C sample contained a void volume fraction below 1% which demonsrates consistent results with the initial motivation of the study. However, it may be demonstrated that the process parameters recommended by the manufacturer are not optimal for multilayer prepregs and the need to revise the process parameters, specifically the vacuum dwell time prior to the curing reaction, because of the fact that sample D could not demonstrate results as successful as sample C with regards to the void volume fraction.

Table 3.6 The evolution of void content, average ply thickness and fiber volume fraction for each sample

Parameters \ Samples	A	B	C	D
Process Condition	Uncured & Uncompacted	Uncured & Compacted	Cured & Compacted	Cured & Compacted
Void content (%)	17.6	5.9	0.88	3.1
Average ply thickness (mm)	0.5	0.72	0.3	0.69
Fiber volume fraction (%)	33.5	48.9	67.59	61.63

3.2 Permeability Characterization

The permeability value pertains to the fiber architecture (or textile type) inputted into the subsequent mathematical modeling significantly influences the resin dispersion within the fiber bed. The resin penetrates the dry regions in accordance with the permeability of the domain [16].

3.2.1 Permeability Modeling

In this study, the transverse flow of the air was considered and the characterization approach included the evaluation of the corresponding element of the permeability tensor. Previously demonstrated CT scans were taken into consideration to establish the model domain which can be regarded as micro-scale, having the dimensions of 0.05 mm x 0.05 mm. The domain shown in Figure 3.6 includes packed-fibers surrounded by void regions, and were confirmed by the scans that they could be considered as the representation of the real fiber stacking. Fiber volume fraction value of the Sample A was taken as reference for the fiber volume fraction of the model domain.

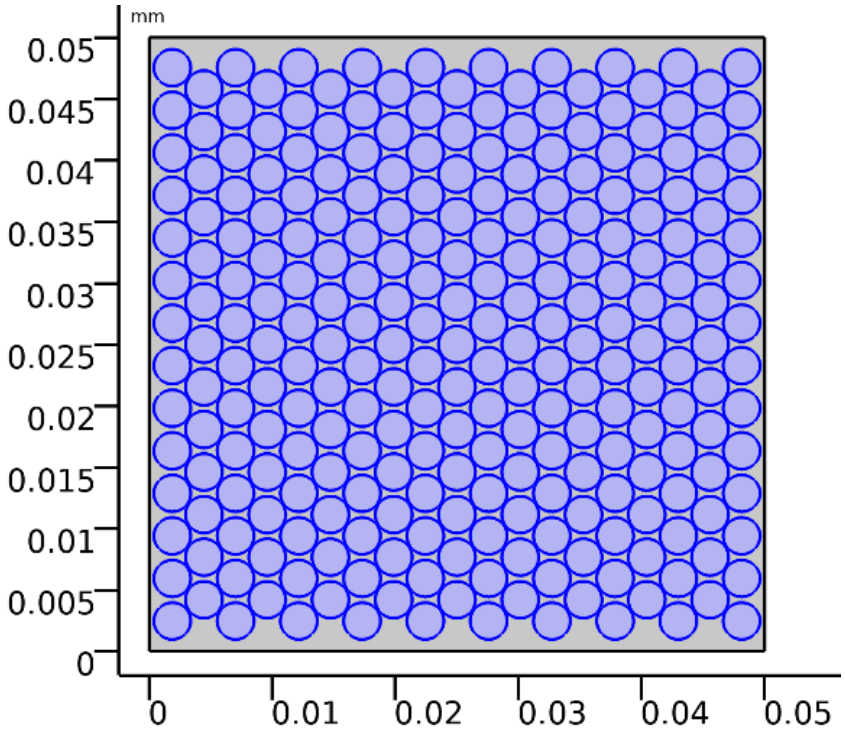

Figure 3.6 Micro-scale model domain where permeability characterization was performed: Fibers (dark circles) and voids (light areas)

In this micro-scale model, the permeability value in the flow direction was calculated by integrating the flow resulted due to pressure difference applied from upper to lower boundaries of the domain with Darcy's Law. The model was based on the Navier-Stokes equation where the fluid is subjected to a body force F, and the Navier-Stokes equation can be written in Equation 3.3 as follows

$$\rho \times [\frac{d\overrightarrow{v}}{dt} + \overrightarrow{v} \times \nabla \overrightarrow{v}] = \rho \times \overrightarrow{F} + \nabla \times \sigma \tag{3.3}$$

Where ρ represents the density, v velocity, t time, P pressure and F volumetric force. In fluid mechanics, permeability is a measure of the ability of a porous material to allow fluid to pass through this porous medium [59]. The most commonly used equation to describe the flow through porous media is Darcy's equation [2]. Fluids modeled based on Darcy's Law (Equation 3.4) must comply with the assumptions adopted to formulate the Navier Stokes equation. That is, fluids must have a constant density and viscosity, and abide by Newtonian behavior [33].

$$K = \frac{\mu \times H \times U_D}{\Delta P} \tag{3.4}$$

Where μ is the viscosity of the liquid, ΔP is the pressure difference, K is the permeability tensor of the porous medium, U_D is the velocity of the fluid, and H is the depth of the cell.

The Reynolds number of the flow should be kept low enough to keep the effects of inertial terms negligible. Reynolds number equation (Equation 3.5) ranges from 1 to 10 ($1 < Re < 10$) [59], where D_e is the pore diameter equivalence.

$$Re = \frac{\rho \times U_D \times D_e}{\mu} \tag{3.5}$$

The porosity is defined as the ratio of volume of the pores to the total volume of representative slice of the porous media; can be calculated using the equation below.

$$\varepsilon = 1 - \frac{N \times \pi \times d^2}{4 \times S_t} \tag{3.6}$$

Where N is the number of fibers, d is the fiber diameter and S_t is the total surface of the unit cell. Thus, "selected viscosity" of a selected air, filling time can be obtained from the simulation at a selected porosity and at a predefined inlet and outlet pressures. Permeability was able to be calculated using Equation 3.4 The permeability calculation was performed using a simulation in which the parameters listed in Table 3.7 were input using the "Creeping Flow" module of the COMSOL Multiphysics® finite element analysis program.

Table 3.7 Required parameters for the permeability analysis

Parameter	Value
Flow equation	Navier-Stokes equation (incompressible, steady-state)
Fiber diameter	6 μm
Unit cell dimensions	0.05 mm x 0.05 mm
Cylinder boundary conditions	No-slip ($u = 0$)
Outer boundary conditions (Left-right)	Slip ($u\ xn = 0$)
Pressure difference (Top-bottom)	1000 Pa

3.2.2 Results and Discussion

The generated mesh within the domain for this CFD study can be examined in Figure 3.7. The velocity field distribution obtained as a result of the study, which is the necessary parameter for the permeability calculation, is depicted in Figure 3.7.

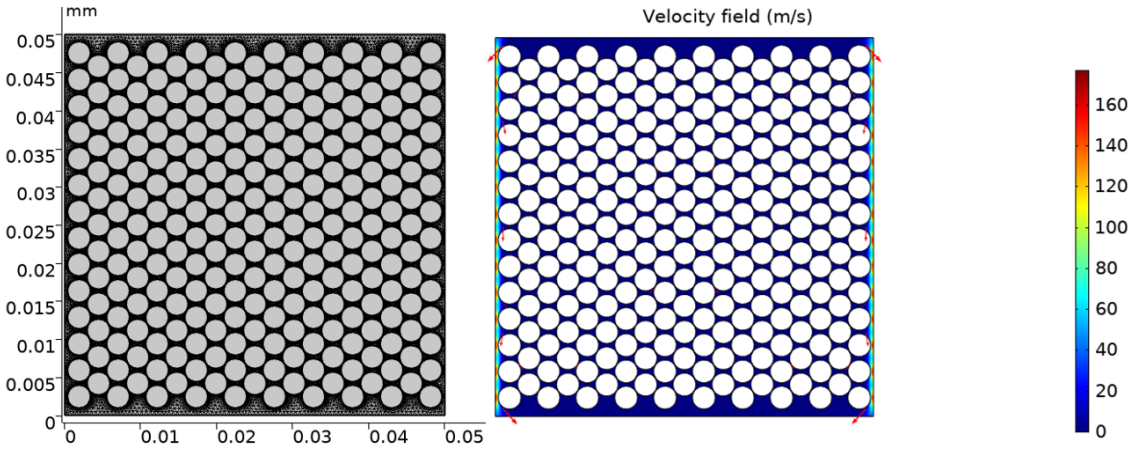

Figure 3.7 The generated mesh for permeability analysis (left) and velocity field distribution (right)

As depicted in Figure 3.8, the permeability value of the airflow between fibers in this micro-scale model was calculated as $2.02x10^{-15}\ m^2$. This value could be defined as the initial permeability in the subsequent mathematical modeling. Characterization of the permeability tensor with this numerical method is accepted in the literature [21, 60–62], and the results can be confirmed with the experimental data.

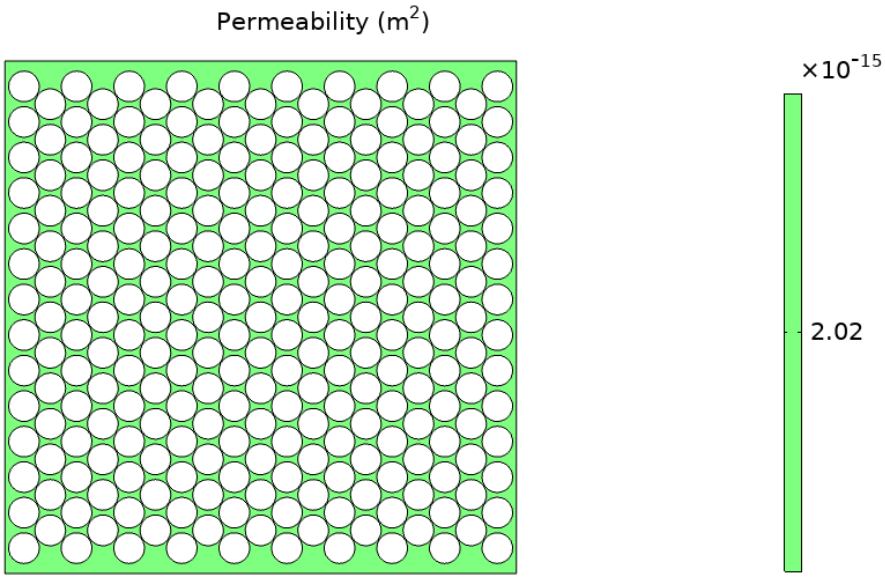

Figure 3.8 The result of micro-scale permeability model

3.3 Thermal Properties

A series of experiments is performed for the prepreg system through the DSC experiments for the resin and prepreg systems to model the heat capacity of the constituents and thermal constant analyzer (TCA) to measure the in-plane and through-thickness thermal conductivities as a function of temperature. Thus, the influence and evolution of these heat properties during the cure can be considered as the inputs of the subsequent process modeling. The following sections will present the specific heat capacity and thermal conductivity of the prepreg system. The experimental procedure and numerical models and the results will be evaluated in detail.

3.3.1 Specific Heat Capacity (C_p)

During the Vacuum Bag Only (VBO) process, specific heat capacity (C_p) of the prepreg system should be accurately characterized since this parameter has distinctive effects on thermal behavior of the prepreg system and incorporate it into the

heat transfer model along with other parameters such as degree of cure and viscosity. Following subsections presents the experimental procedure and specific heat capacity model and the results

3.3.1.1 Experimental Work

Dynamic Scanning Calorimeter (DSC) is one of the commonly preferred apparatus to measure the heat capacity of the materials [55] (see Figure 2.2). As stated above, specific heat capacity of the complete prepreg system and the resin system itself were distinctively characterized. Specific heat capacity (C_p) values were obtained by several sets of experiments performed by a Mettler Toledo DSC 3+ differential scanning calorimeter (DSC) [30]. Measurements were performed at a temperature range of -60 to 350°C with a heating rate of 10°C/min in dynamic conditions. Table 3.8 summarizes the test matrix to characterize the specific heat capacities in this study. As suggested in the literature [54], the DSC instrument was calibrated with a well-known reference material, a sapphire sample, within the same temperature range with a similar heating rate before each test. DSC experiments were repeated three times.

Table 3.8 Specific heat capacity (C_p) characterization test matrix

Sample	Test Type	Temperature Range (°C)	Heat Rate (°C/min)	No. Tests
KOM12 Prepreg System	Dynamic	-60 to 350	10	3
OM12 Epoxy/Resin System			10	3

3.3.1.2 C_p Modeling

DSC apparatus measures the heat flux (dH/dt) during the temperature ramp (dT/dt) and it is usually a function of temperature with a constant slope. Therefore, a linear regression is often sufficient to predict the step change in specific heat capacity of the resin system during the curing period (80-130°C) for OM12 resin system). However, since T_g is slightly an endothermic reaction the slope may differ between before/after T_g of the resin system. Hence, linear regression was applied over a temperature range of 20-220°C to accurately predict the specific heat capacity behavior of the materials.

Furthermore, in this study, the commonly used rule of mixture method [63] based on the weight fractions (Equation 3.7) was preferred and applied to prepreg and resin system results to predict the specific heat capacity of the reinforcement system.

$$C_{p_c} = m_f C_{p_f} + m_r C_{p_r} \tag{3.7}$$

where C_{p_c}, C_{p_f} and C_{p_r} represent the specific heat capacities of the composite, fiber and resin, respectively.

3.3.1.3 Results and Discussion

Figure 3.9 depicts the specific heat capacity values of the prepreg system constituents, predicted using a rule of mixtures model for specific heat capacity and linear regression. The results revealed that the specific heat capacity of the constituents exhibited a noticeable increase following a linear trend.

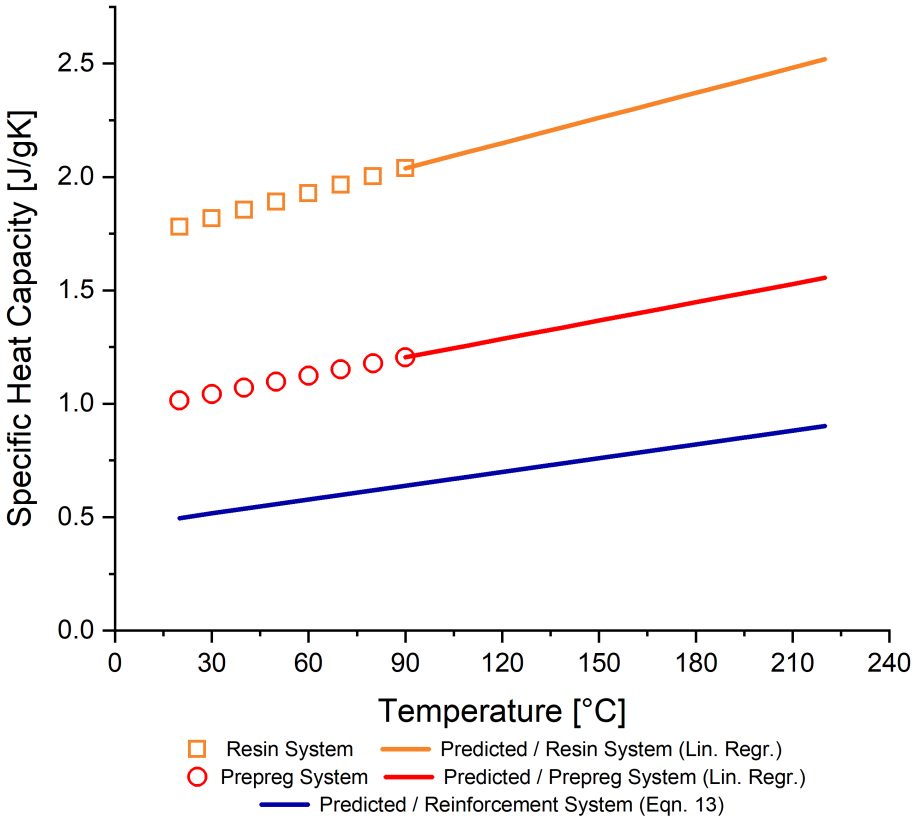

Figure 3.9 Final predicted specific heat capacity values of the constituent materials

3.3.2 Thermal Conductivity (k)

The thermal conductivity of the resin and fiber components of the prepreg could be investigated individually by certain thermal conductivity models [55]. For the thermal conductivity experiments, complete prepreg system and epoxy resin composition of the prepreg itself were used. Following subsections describe the experimental procedure, adapted models and the results of this thermal conductivity characterization study.

3.3.2.1 Experimental Work and Results

In this study, the thermal conductivity of the complete prepreg system and the resin itself were characterized in different temperatures to obtain the intrinsic thermal conductivities of the components. In addition to the effects due to geometrical disposition and fiber/resin fraction, thermal conductivity is a temperature dependent property which means that the material can demonstrate different thermal conductivity behavior in different temperature conditions. In order to clarify this statement, there conducted different sets of experiments at several temperature points. According to the literature, although, thermal conductivity is a temperature dependent property, it varies slightly in a limited temperature range [55]. Therefore, it was planned to conduct the experiments in a wide temperature range to observe the noticeable differences in the thermal conductivity of the materials. However, the prepreg system used in this study composes of a fast cure resin with a cure cycle between 80-130°C. Hence, 2 sets of experiments were performed prior to cure cycle, Table 3.9 summarizes the completed experiments.

Table 3.9 Thermal conductivity characterization test matrix

Sample	Ambient Temperature (C)	No. Tests
KOM12 Prepreg System	25	4
	60	4
OM12 Epoxy Resin System	25	3
	60	3

There are two categories of methods for the thermal conductivity measurements: steady-state and transient (non-steady-state) methods. The commonly preferred steady-state method is based on Fourier's Law of heat conduction. In this method, the sample is placed between hot and cold two plates with a constant heat flux in order to maintain the steady-state condition. However, in this method the required time period to reach the steady state condition is considerably long even for a thin composite plate. Transient Plane Source Method (TPS) can be given as an example for the non-steady-state methods. In this method, a thin-flat (film type) sensor is placed between two identical samples, the heat is generated and dissipated from both sides of the sensor into the samples and time-temperature signal is recorded. Figure 3.10 depicts the operation principle of the experiments based on the transient plane source method.

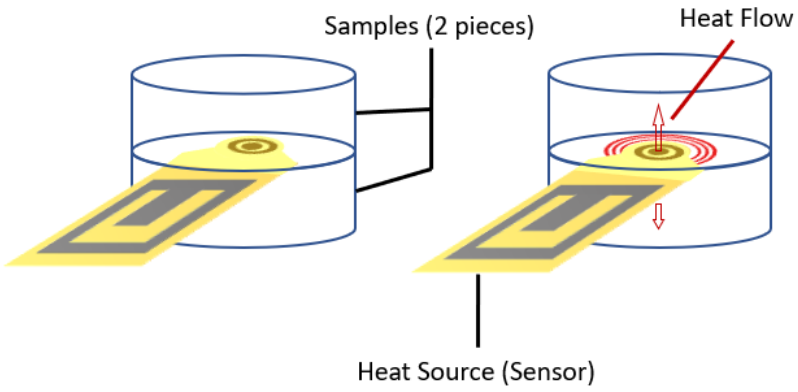

Figure 3.10 Operation principle of the sensor for the thermal conductivity characterization based on Transient Plane Source (TPS) Method

In this study, a novel experimental strategy was developed to characterize the prepreg system's thermal conductivity and its constituents. Figure 3.11 represents the experiment overview performed for the complete prepreg system. Measurements were carried out with a thermal constant analyzer, Hot Disk (TPS 2500S model), and an oven to maintain the determined temperature of the experiment medium as previously demonstrated in the literature [64]. The setup was installed in an oven with a sensor placed between two rolled prepreg samples stacked with the same fiber configuration (UD - 0°) to constitute the isothermal setting for the sensor. For the first set of experiments, the prepreg samples were prepared as follows; 5 layers of 30 x 30 cm fiber orientation, and then the prepreg stack was rolled in parallel to the unidirectionally aligned fibers to form a cylinder. Next, the rolled sample was cut into 2 identical pieces by a water jet cutter in order to avoid distracting the fiber orientations. Subsequently, two cylindrical samples with the dimensions of 50 mm diameter and 50 mm height were obtained. As previously stated, a sensor was placed between two samples and they were installed into a pressing mechanism to avoid the gap between the sensor and samples. In this method, there are two assumptions that were already admitted by the test equipment while performing the experiment: the UD fibers are perfectly aligned in-line, and distractions within the fiber orientations were successfully avoided which means that UD fibers of two samples are perfectly matched during the test.

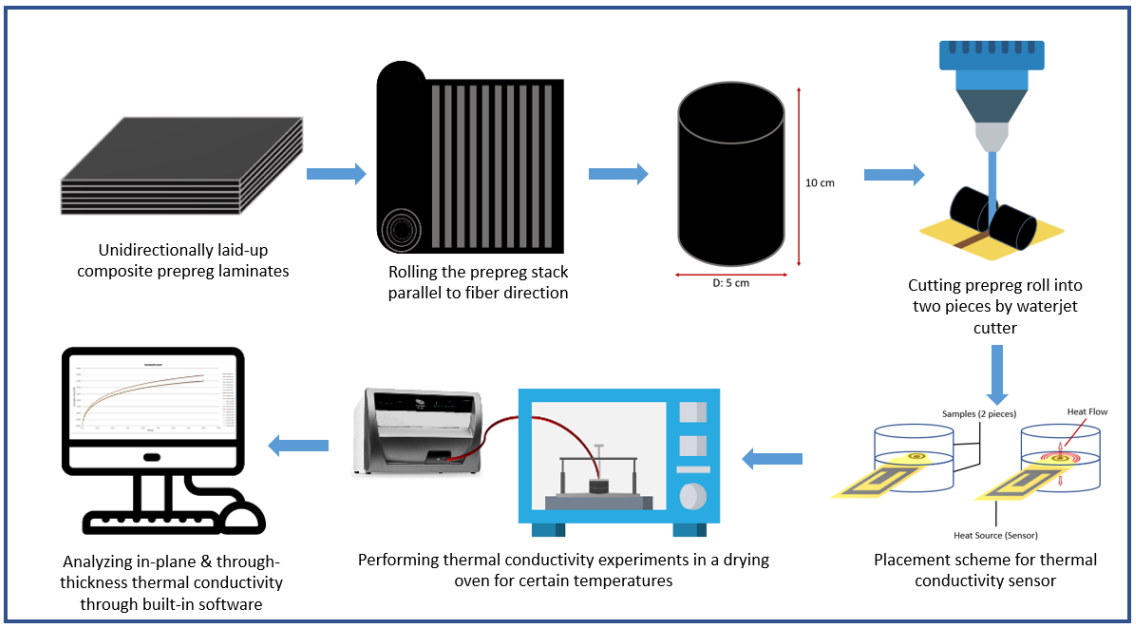

Figure 3.11 Experiment steps of thermal conductivity characterization for the complete prepreg system

Additionally, the equipment requires the specific heat capacity of the sample (C_p) to be inputted as in MJ/m^3K unit and therefore, the (C_p) values of the samples obtained in the DSC experiments explained in the previous section were converted from J/gK into MJ/m^3K. The equipment provided two different thermal conductivity results as axial and radial thermal conductivity values. As for the thermal conductivity tensor for this experiment method it may be noted as follows:

$$k = \begin{bmatrix} k_{xx} & 0 & 0 \\ 0 & k_{yy} & 0 \\ 0 & 0 & k_{zz} \end{bmatrix} \tag{3.8}$$

$$k_{xx} = k_{axial} \tag{3.9}$$

$$k_{yy} = k_{zz} = k_{radial} \tag{3.10}$$

As for the thermal conductivity characterization of the resin system the OM12 the epoxy resin was removed from the freezer where it is stored at -18°C and kept at room temperature in order the resin can liquify. Later, a small portion of resin the resin was loaded upon flat surface of the sensor with a diameter of 50 mm and height of at least 10 mm. Subsequently, the sensor was placed in a drying

oven to maintain the predetermined temperature of the experiment medium. In this experiment, the equipment provided a single thermal conductivity value for both in-plane and through-thickness directions due to isotropy of the resin system. Table 3.10 summarizes the anisotropic thermal conductivity results in axial and radial directions for the prepreg samples and isotropic thermal conductivity results for the resin material obtained from the experiments performed at 25 and 60°C.

Table 3.10 Anisotropic/Isotropic thermal conductivity results of the experiments

Samples / Parameters	Ambient Temperature (°C)	k_{axial} (W/mK)	k_{radial} (W/mK)
KOM12 Prepreg System	25	5.5444	0.44439
	60	6.5199	0.41319
OM12 Epoxy Resin System	25	0.1934	
	60	0.1549	

3.3.2.2 k Modeling

As stated in the previous subsection, the prepreg used in this study has anisotropic thermal conductivity due to its composition and the alignment of the reinforcement material (fiber). Anisotropy of the prepreg system leads to different thermal gradients in accordance with the heat flow through different fiber directions [64]. Therefore, there is an obvious need for mathematical models to predict the thermal conductivity of both resin and reinforcement material of the prepreg system. For unidirectional composites, the commonly adopted thermal conductivity models were developed by Springer and Tsai [63] for the in-plane, $k_{||}$, (along the fibers) and transverse, $k_{\perp}$, (perpendicular to the fibers) directions as described below. k_r&k_f, v_r&v_f are the thermal conductivities and volume fractions of the resin and fiber, respectively.

$$k_{||} = v_r k_r + v_f k_f \tag{3.11}$$

$$k_{\perp} = \frac{1}{\frac{v_f}{k_f} + \frac{v_r}{k_r}} \tag{3.12}$$

3.3.2.3 Results and Discussion

Anisotropic thermal conductivity (in-plane & through-thickness) for the prepreg system and isotropic thermal conductivity values for the matrix (resin) material were obtained from the experiments performed at 25 and 60°C. It should be noted that k_{axial} corresponds to in-plane $\left(k_{||}\right)$ and k_{radial} corresponds to through-thickness $(k_{\perp})$ thermal conductivities due to geometrical installment of the rolled prepreg halves in the experimental setup (see Figure 3.11). Additionally, it is already known that volume fractions of the constituents for resin and reinforcement materials as follow; $v_r = 0.343$ and $v_f = 0.322$, respectively. Thus, thermal conductivity values of each constituent were calculated by applying the mathematical model explained above and summarized in Table 3.11

Table 3.11 Calculated thermal conductivity results of the reinforcement system

Samples / Parameters	Ambient Temperature (°C)	k_{axial} (W/mK)	k_{radial} (W/mK)
Reinforcement System	25	17.013	0.6756
	60	20.083	1.5647

Comparison of the findings with those of other studies confirms [55, 63] that the thermal conductivity values do not demonstrate a noteworthy change with the temperature. Therefore, the values obtained through these experiments can be considered as the reference values for the prepreg system thermal conductivity.

3.4 Summary

The main material properties and processing parameters of the KOM12 prepreg system were characterized and detailed following a systematic in this chapter. This involved several sets of experiments using optical microscopy, micro-CT, DSC, and TCA apparatus to investigate fiber architecture, the change in fiber volume fraction, void content, and the evolution of thermal properties such as specific heat capacity and thermal conductivity. Micro-CT was found to accurately characterize the prepreg system in regards to void content, fiber volume fraction change in stages of the curing process, and geometry and location of the dry fiber-tow areas. These

experiments also provided the necessary data for the subsequent CFD modeling to predict the micro-scale initial permeability of the prepreg system.

Additionally, the specific heat capacity of the prepreg and its constituents was modeled as a function of temperature using a fitting approach coupled with DSC runs. The correlation between specific heat capacity and the temperature is worth noting because specific heat capacity almost doubled during the heat-up.

Finally, a novel experimental strategy was developed to characterize the prepreg system's thermal conductivity and its constituents. One of the most important findings of this study was that thermal conductivity values do not demonstrate a significant change with the temperature.

Together with the characterization methods for the resin system, the main material properties, and processing parameters of the VBO prepreg system were characterized.

4. CONCLUSIONS AND FUTURE WORKS

In this thesis, a comprehensive methodology was developed that systematically characterizes material properties and the constitutive behavior of a VBO prepreg system to invigorate the VBO prepreg process model and increase its accuracy. To achieve this goal, this methodology was implemented to characterize a commercial VBO prepreg system's material properties and main processing parameters.

First, the cure-dependent properties of the epoxy resin were characterized to predict the cure kinetics, rheology, and glass transition temperature behavior under vacuum-bag-only cure conditions. The cure-dependent model parameters were obtained by adopting the least-squares methods to fit the experimental data determined through DSC, rheometer, and DMA, respectively. For this, a diffusion-controlled cure kinetics model accurately predicted the cure kinetics behavior of the epoxy resin and exhibited excellent agreement with the dynamic and isothermal DSC experiments. Subsequently, a phenomenological viscosity model was implemented to successfully estimate the resin rheological behavior driven by the temperature and degree of cure. It was demonstrated that the model resulted a reasonable agreement with the rheology experiments at different dynamic conditions. Finally, the DiBenedetto equation was employed to describe the glass transition temperature evolution of the epoxy resin system with the degree of cure.

Second, first fiber architecture was investigated as the main microstructural evolution is the resin flow into dry regions. The resulting micrographs exhibited that the domain wherein resin flow and air evacuation occur consisted of elliptical dry fiber tow areas, containing randomly packed fibers, surrounded by resin-rich regions. This was followed by void-content, and the fiber volume fraction analyses of the prepreg system through sets of x-ray tomography scans of the laminates processed to different stages of curing. Representative micro slices were subjected to different 2d and 3d analysis to predict the void content change and evolution of fiber volume fraction. It was revealed that initially dry fiber tow areas were considerably shrunk as they were infiltrated by the resin and identified as air evacuation channels. It was also observed that the macro-voids present between prepreg plies diminish as the laminates

were subjected to consolidation and vacuum during the curing process. On the other hand, the fiber volume fraction was found to significantly increase subsequent to the consolidation and air evacuation, and stabilize after the resin reaches the gelation. This highlighted the importance of the application of consolidation and debulking on the purpose of eliminating inter-ply gaps. Furthermore, microscopic transverse permeability of the fabric was calculated through a CFD simulation performed for a micro-scale domain consisting of random packs of fibers and resin-rich regions. This predicted permeability value then can be inputted as an initial permeability value for the subsequent mathematical modeling and numerical analysis.

Third, specific heat capacity and thermal conductivity of the prepreg system constituents were characterized to better describe the heat transfer of the laminates during the VBO prepreg processing and include them into the integrated process model to be established. A series of experiments were performed through DSC and TCA to predict the evolution of specific heat capacity and thermal conductivity of the prepreg system with the temperature, respectively. Thus, the evolution of these two fundamental thermal properties and their effects on the heat transfer of the system were able to be characterized and incorporated into the subsequent process modeling.

Finally, the devised approach can be accepted as a starting point towards establishing a methodology of process design that integrates characterization, modeling, optimization, and verification to produce high-performance composite structures through OoA techniques with allowed void content.

Future Works

This thesis's present findings might suggest several courses of action for future works, outlined below:

- Changes in the model and parameters may be considered to increase accuracy further.
- For the viscosity model, isothermal experiments should be repeated with consistent experiment parameters, and the equation can be fitted to both dynamic and isothermal experiments. Hence, the accuracy of the model can be improved.
- This research could potentially lead to further studies to adapt this systematic methodology to characterize the thermoplastic prepreg systems.
- This study has gone some way towards enhancing the understanding of vacuum bag only prepregs and their constitutive material properties to produce high-performance composite structures through OoA techniques with allowed void content. Further studies could focus on establishing a systematic and overarching methodology of process design that integrates characterization, modeling, optimization, and verification altogether.

Bibliography

[1] F. C. Campbell. *Manufacturing Processes for Advanced Composites*. 2003. ISBN: 9781856174152. DOI: 10.1016/B978-1-85617-415-2.X5000-X.

[2] Suresh G. Advani and E. Murat Sozer. "Constitutive Laws and Their Characterization". In: *Process Modeling in Composites Manufacturing*. Boca Raton: CRC Press, 2003. DOI: 10.1201/9780203910061.

[3] Flake Campbell. *Manufacturing Technology for Aerospace Structural Materials*. 2006. ISBN: 9781856174954. DOI: 10.1016/B978-1-85617-495-4.X5000-8.

[4] T. Centea and P. Hubert. "Out-of-autoclave prepreg consolidation under deficient pressure conditions". In: *Journal of Composite Materials* (2014). ISSN: 1530793X. DOI: 10.1177/0021998313494101.

[5] T. Centea, L. K. Grunenfelder, and S. R. Nutt. "A review of out-of-autoclave prepregs - Material properties, process phenomena, and manufacturing considerations". In: *Composites Part A: Applied Science and Manufacturing* 70 (2015), pp. 132–154. ISSN: 1359835X. DOI: 10.1016/j.compositesa.2014.09.029.

[6] Ginger Gardiner. *Out-of-autoclave prepregs: Hype or revolution?* 2011. URL: https://www.compositesworld.com/articles/out-of-autoclave-prepregs-hype-or-revolution.

[7] Jeff Sloan. *Out-of-autoclave processing: <1% void content?* 2015. URL: https://www.compositesworld.com/articles/out-of-autoclave-processing-1-void-content.

[8] Göran Fernlund, Christophe Mobuchon, and Navid Zobeiry. "2.3 Autoclave Processing". In: 2018.

[9] L. K. Grunenfelder and S. R. Nutt. "Void formation in composite prepregs - Effect of dissolved moisture". In: *Composites Science and Technology* (2010). ISSN: 02663538. DOI: 10.1016/j.compscitech.2010.09.009.

[10] N. Bernet et al. "Commingled yarn composites for rapid processing of complex shapes". In: *Composites - Part A: Applied Science and Manufacturing* (2001). ISSN: 1359835X. DOI: 10.1016/S1359-835X(00)00180-9.

[11] Timothy George Peter Gutowski and Timothy George Peter Gutowski. *Advanced composites manufacturing*. Vol. 1. Wiley New York, 1997.

[12] Ling Liu et al. "Effects of cure cycles on void content and mechanical properties of composite laminates". In: *Composite Structures* (2006). ISSN: 02638223. DOI: 10.1016/j.compstruct.2005.02.001.

[13] T. Centea and P. Hubert. “Measuring the impregnation of an out-of-autoclave prepreg by micro-CT”. In: *Composites Science and Technology* 71.5 (2011), pp. 593–599. ISSN: 02663538. DOI: 10.1016/j.compscitech.2010.12.009.

[14] J Boyd. “Vacuum Bag only Composite Part Manufacturing (Tutorial Handout)”. In: *SAMPE 2003 Technical Conference*. Dayton, OH, 2003, p. 72.

[15] Mark Steele and Tom Corden. “New Prepregs for Cost Effective, Out-of-Autoclave Tool and Component Manufacture.” In: *SAMPE journal* 40.2 (2004), pp. 30–34.

[16] T. Centea and P. Hubert. “Modelling the effect of material properties and process parameters on tow impregnation in out-of-autoclave prepregs”. In: *Composites Part A: Applied Science and Manufacturing* 43.9 (2012), pp. 1505–1513. ISSN: 1359835X. DOI: 10.1016/j.compositesa.2012.03.028.

[17] Mahoor Mehdikhani et al. *Voids in fiber-reinforced polymer composites: A review on their formation, characteristics, and effects on mechanical performance*. 2019. DOI: 10.1177/0021998318772152.

[18] J. Kardos, M. Duduković, and R. Dave. “Void growth and resin transport during processing of thermosetting - Matrix composites - Epoxy Resins and Composites IV - Advances in Polymer Science”. In: *Advances in Polymer Science* (1986). ISSN: 0065-3195. DOI: 10.1007/3-540-16423-5_13.

[19] Theodosia Kourkoutsaki et al. “A process modeling toolkit developed to address scale-up challenges of out-of-autoclave manufacturing”. In: *CAMX 2015 - Composites and Advanced Materials Expo* October (2015), pp. 2434–2450.

[20] John J. Gangloff, Wook R. Hwang, and Suresh G. Advani. “Characterization of bubble mobility in channel flow with fibrous porous media walls”. In: *International Journal of Multiphase Flow* (2014). ISSN: 03019322. DOI: 10.1016/j.ijmultiphaseflow.2013.12.003.

[21] Hatice S. Sas et al. “Thermoset Pultrusion Process: Modeling and Experimental Characterization”. In: *Proceedings of CAMX conference*. Orlando, 2014.

[22] Pascal Hubert and Anoush Poursartip. “A review of flow and compaction modelling relevant to thermoset matrix laminate processing”. In: *Journal of Reinforced Plastics and Composites* 17.4 (1998), pp. 286–318.

[23] A Yousefi, PG Lafleur, and R Gauvin. “Kinetic studies of thermoset cure reactions: a review”. In: *Polymer Composites* 18.2 (1997), pp. 157–168.

[24] Loleï Khoun. “Process-induced stresses and deformations in woven composites manufactured by resin transfer moulding”. PhD thesis. McGill University Montreal, 2009.

[25] James Kratz. “Processing composite sandwich structures using out-of-autoclave technology”. PhD thesis. McGill University MSc thesis, 2009.

[26] Timotei Centea. “Material-Processing-Quality Relationships During the Consolidation of Out-of Autoclave Prepregs”. PhD thesis. McGill University Libraries, 2013.

[27] P. Hubert et al. “Cure kinetics and viscosity models for Hexcel 8552 epoxy resin”. In: *International SAMPE Symposium and Exhibition (Proceedings)*. 2001.

[28] Sung-Nung Lee, Ming-Tsung Chiu, and Ho-Sheng Lin. “Kinetic model for the curing reaction of a tetraglycidyl diamino diphenyl methane/diamino diphenyl sulfone (TGDDM/DDS) epoxy resin system”. In: *Polymer Engineering & Science* 32.15 (1992), pp. 1037–1046.

[29] Loleï Khoun, Timotei Centea, and Pascal Hubert. “Characterization methodology of thermoset resins for the processing of composite materials -Case study”. In: *Journal of Composite Materials* 44.11 (2010), pp. 1397–1415. ISSN: 00219983. DOI: 10.1177/0021998309353960.

[30] James Kratz et al. “Thermal models for MTM45-1 and Cycom 5320 out-of-autoclave prepreg resins”. In: *Journal of Composite Materials* 47.3 (2013), pp. 341–352. ISSN: 00219983. DOI: 10.1177/0021998312440131.

[31] M. R. Kamal and S. Sourour. “Kinetics and thermal characterization of thermoset cure”. In: *Polymer Engineering & Science* 13.1 (1973), pp. 59–64. ISSN: 15482634. DOI: 10.1002/pen.760130110.

[32] K. C. Cole, J. J. Hechler, and D. Noël. “A New Approach to Modeling the Cure Kinetics of Epoxy Amine Thermosetting Resins. 2. Application to a Typical System Based on Bis[4-(diglycidylamino)phenyl]methane and Bis(4-aminophenyl) Sulfone”. In: *Macromolecules* 24.11 (1991), pp. 3098–3110. ISSN: 15205835. DOI: 10.1021/ma00011a012.

[33] S. Amico and C. Lekakou. “Mathematical modelling of capillary micro-flow through woven fabrics”. In: *Composites Part A: Applied Science and Manufacturing* (2000). ISSN: 1359835X. DOI: 10.1016/S1359-835X(00)00033-6.

[34] MARK J. PARKER. “Test Methods for Physical Properties”. In: *Comprehensive Composite Materials* 5 (2000), pp. 183–226. DOI: 10.1016/b0-08-042993-9/00074-7.

[35] J. M. Castro and C. W. Macosko. “KINETICS AND RHEOLOGY OF TYPICAL POLYURETHANE REACTION INJECTION MOLDING SYSTEMS.” In: *Society of Plastics Engineers (Technical Papers)*. 1980.

[36] JP Pascault and RJJ Williams. “Glass transition temperature versus conversion relationships for thermosetting polymers”. In: *Journal of Polymer Science Part B: Polymer Physics* 28.1 (1990), pp. 85–95.

[37] Daniel J. O’Brien and Scott R. White. “Cure Kinetics, Gelation, and Glass Transition of a Bisphenol F Epoxide”. In: *Polymer Engineering and Science* 43.4 (2003), pp. 863–874. ISSN: 00323888. DOI: 10.1002/pen.10071.

[38] Sindee L Simon, Gregory B Mckenna, and Olivier Sindt. “Modeling the evolution of the dynamic mechanical properties of a commercial epoxy during cure after gelation”. In: *Journal of Applied Polymer Science* 76.4 (2000), pp. 495–508.

[39] Patricia Prasatya, Gregory B McKenna, and Sindee L Simon. “A viscoelastic model for predicting isotropic residual stresses in thermosetting materials: effects of processing parameters”. In: *Journal of Composite Materials* 35.10 (2001), pp. 826–848.

[40] J Magnus Svanberg and J Anders Holmberg. “Prediction of shape distortions Part I. FE-implementation of a path dependent constitutive model”. In: *Composites part A: applied science and manufacturing* 35.6 (2004), pp. 711–721.

[41] Jelena Muric-Nesic, Paul Compston, and ZH Stachurski. “On the void reduction mechanisms in vibration assisted consolidation of fibre reinforced polymer composites”. In: *Composites Part A: Applied Science and Manufacturing* 42.3 (2011), pp. 320–327.

[42] C Santulli et al. “Void content measurements in commingled E-glass/polypropylene composites using image analysis from optical micrographs”. In: *Science and engineering of composite materials* 10.2 (2002), pp. 77–90.

[43] Danning Zhang. “Void consolidation of thermoplastic composites via non-autoclave processing”. PhD thesis. University of Delaware, 2017.

[44] F. Y.C. Boey and S. W. Lye. “Void reduction in autoclave processing of thermoset composites. Part 1: High pressure effects on void reduction”. In: *Composites* (1992). ISSN: 00104361. DOI: 10.1016/0010-4361(92)90186-X.

[45] P. Olivier, J.P. Cottu, and B. Ferret. “Effects of cure cycle pressure and voids on some mechanical properties of carbon/epoxy laminates”. In: *Composites* 26.7 (1995), pp. 509–515. ISSN: 0010-4361. DOI: 10.1016/0010-4361(95)96808-J. URL: https://www.sciencedirect.com/science/article/abs/pii/001043619596808J.

[46] S. Sequeira Tavares, V. Michaud, and J. A.E. Månson. “Through thickness air permeability of prepregs during cure”. In: *Composites Part A: Applied Science and Manufacturing* (2009). ISSN: 1359835X. DOI: 10.1016/j.compositesa.2009.07.004.

[47] Jackson K and Crabtree M. “Autoclave quality composites tooling for composite from vacuum bag only processing.” In: *47th International SAMPE Symposium and Exhibition*. 2002, pp. 800–807.

[48] J J Gangloff Jr. et al. “In situ flow visualization of void migration during Out-of-Autoclave thermoset prepreg processing”. In: *Proceedings of the 12th International Conference on Flow Processes in Composite Materials* (2014).

[49] John J. Gangloff et al. “Entrapment and venting of bubbles during vacuum bag prepreg processing”. In: *Journal of Composite Materials* (2017). ISSN: 1530793X. DOI: 10.1177/0021998316676325.

[50] R. Helmus, R. Hinterhölzl, and P. Hubert. “A stochastic approach to model material variation determining tow impregnation in out-of-autoclave prepreg consolidation”. In: *Composites Part A: Applied Science and Manufacturing* 77 (2015), pp. 293–300. ISSN: 1359835X. DOI: 10.1016/j.compositesa.2015.03.021. URL: http://dx.doi.org/10.1016/j.compositesa.2015.03.021.

[51] Seong Soon Hwang et al. “Cure kinetics and viscosity modeling for the optimization of cure cycles in a vacuum-bag-only prepreg process”. In: *International Journal of Advanced Manufacturing Technology* 99.9-12 (2018), pp. 2743–2753. ISSN: 14333015. DOI: 10.1007/s00170-018-2467-y.

[52] S. Hernández et al. “Effect of curing cycle on void distribution and interlaminar shear strength in polymer-matrix composites”. In: *Composites Science and Technology* (2011). ISSN: 02663538. DOI: 10.1016/j.compscitech.2011.05.002.

[53] L. K. Grunenfelder et al. “Effect of room-temperature out-time on tow impregnation in an out-of-autoclave prepreg”. In: *Composites Part A: Applied Science and Manufacturing* 45 (2013), pp. 119–126. ISSN: 1359835X. DOI: 10.1016/j.compositesa.2012.10.001.

[54] Bernd Weidenfeller, Michael Höfer, and Frank R. Schilling. “Thermal conductivity, thermal diffusivity, and specific heat capacity of particle filled polypropylene”. In: *Composites Part A: Applied Science and Manufacturing* 35.4 (2004), pp. 423–429. ISSN: 1359835X. DOI: 10.1016/j.compositesa.2003.11.005.

[55] Lei Shi. “Heat Transfer in the Thick Thermoset Composites”. PhD Dissertation. PhD Thesis, Northwestern Polytechnical University, 2016, pp. 1 –127. ISBN: 9789462954595.

[56] Georgios Kalogiannakis, Danny Van Hemelrijck, and Guy Van Assche. “Measurements of thermal properties of carbon/epoxy and glass/epoxy using modulated temperature differential scanning calorimetry”. In: *Journal of Composite Materials* 38.2 (2004), pp. 163–175. ISSN: 00219983. DOI: 10.1177/0021998304038647.

[57] Jörg Läuger. *Interfacial Shear Rheology of Coffee Samples*. URL: http://www.metrohmsiam.com/foodlab/FL_22/FL22_C22IA108EN-B_Coffee.pdf.

[58] A. T. DiBenedetto. “Prediction of the glass transition temperature of polymers: A model based on the principle of corresponding states”. In: *Journal of Polymer Science Part B: Polymer Physics* (1987). ISSN: 10990488. DOI: 10.1002/polb.1987.090250914.

[59] M Karaki et al. “A comparative analytical, numerical and experimental analysis of the microscopic permeability of fiber bundles in composite materials”. In: *International Journal of Composite Materials* (2017). DOI: 10.5923/j.cmaterials.20170703.02.

[60] M.A. Ali, R. Umer, and K.A. Khan. “A virtual permeability measurement framework for fiber reinforcements using micro CT generated digital twins”. In: *International Journal of Lightweight Materials and Manufacture* (2019). ISSN: 25888404. DOI: 10.1016/j.ijlmm.2019.12.002.

[61] K. Naresh et al. *The use of X-ray computed tomography for design and process modeling of aerospace composites: A review*. 2020. DOI: 10.1016/j.matdes.2020.108553.

[62] Ilya Straumit et al. “Computation of permeability of a non-crimp carbon textile reinforcement based on X-ray computed tomography images”. In: *Composites Part A: Applied Science and Manufacturing* 81 (2016), pp. 289–295. ISSN: 1359835X. DOI: 10.1016/j.compositesa.2015.11.025. URL: http://dx.doi.org/10.1016/j.compositesa.2015.11.025.

[63] George S. Springer and Stephen W. Tsai. “Thermal Conductivities of Unidirectional Materials”. In: *Journal of Composite Materials* 1.2 (1967), pp. 166–173. ISSN: 0021-9983. DOI: 10.1177/002199836700100206.

[64] H. Serkan Tekce, Dilek Kumlutas, and Ismail H. Tavman. “Effect of particle shape on thermal conductivity of copper reinforced polymer composites”. In: *Journal of Reinforced Plastics and Composites* 26.1 (2007), pp. 113–121. ISSN: 07316844. DOI: 10.1177/0731684407072522.